

# Identification of maize genes that condition early systemic infection of sugarcane mosaic virus through single-cell transcriptomics

Xi Chen<sup>1</sup>, Ru Yao<sup>2</sup>, Xia Hua<sup>1</sup>, Kaitong Du<sup>1</sup>, Boxin Liu<sup>2</sup>, Yongxian Yuan<sup>2</sup>, Pei Wang<sup>1</sup>, Qin Yan<sup>1</sup>, Laihua Dong<sup>1</sup>, Simon C. Groen<sup>3,4</sup>, Sanjie Jiang<sup>2,\*</sup> and Tao Zhou<sup>1,\*</sup>

<sup>1</sup>State Key Laboratory of Maize Bio-breeding, Department of Plant Pathology, China Agricultural University, Beijing 100193, China

<sup>2</sup>BGI Genomics, BGI-Shenzhen, Guangdong 518018, China

<sup>3</sup>Department of Nematology and Department of Botany & Plant Sciences, University of California, Riverside, Riverside, CA 92521, USA

<sup>4</sup>Center for Plant Cell Biology, Institute for Integrative Genome Biology, University of California, Riverside, Riverside, CA 92521, USA

\*Correspondence: Sanjie Jiang ([jiangsanjie@genomics.cn](mailto:jiangsanjie@genomics.cn)), Tao Zhou ([taozhoucau@cau.edu.cn](mailto:taozhoucau@cau.edu.cn))

<https://doi.org/10.1016/j.xplc.2025.101297>

## ABSTRACT

During the early systemic infection of plant pathogens, individual cells can harbor pathogens at various stages of infection, ranging from absent to abundant. Consequently, gene expression levels within these cells in response to the pathogens exhibit significant variability. These variations are pivotal in determining pathogenicity or susceptibility, yet they remain largely unexplored and poorly understood. Sugarcane mosaic virus (SCMV) is a representative member of the monocot-infecting potyviruses with a polyadenylated RNA genome, which can be captured by single-cell RNA sequencing (scRNA-seq). Here, we performed scRNA-seq on SCMV-infected maize leaves during early systemic infection (prior to symptom manifestation) to investigate the co-variation patterns between viral accumulation and intracellular gene expression alterations. We identified five cell types and found that mesophyll-4 (MS4) cells exhibited the highest levels of viral accumulation in most cells. Early systemic infection of SCMV resulted in a greater up-regulation of differentially expressed genes, which were mainly enriched in biological processes related to translation, peptide biosynthesis, and metabolism. Co-variation analysis of the altered maize gene expression and viral accumulation levels in MS1, 2, and 4 revealed several patterns, and the co-expression relationships between them were mainly positive. Furthermore, functional studies identified several potential anti- or pro-viral factors that may play crucial roles during the early stage of SCMV systemic infection. These results not only provide new insights into plant gene regulation during viral infection but also offer a foundation for future investigations of host–virus interactions across molecular, cellular, and physiological scales.

**Key words:** systemic infection, differentially expressed genes, co-variation, functional study, anti- or pro-viral factors

**Chen X., Yao R., Hua X., Du K., Liu B., Yuan Y., Wang P., Yan Q., Dong L., Groen S.C., Jiang S., and Zhou T.** (2025). Identification of maize genes that condition early systemic infection of sugarcane mosaic virus through single-cell transcriptomics. *Plant Comm.* **6**, 101297.

## INTRODUCTION

Plant viral systemic infections cause severe damage to crops, which can lead to epidemics and pose serious threats to food security. In plants, viral infection is a dynamic process driven by the interplay between antiviral cellular pathways and viral machinery (Calil and Fontes, 2017; Fontes et al., 2021). Following initial infection, this process progresses through multiple stages. The virus first invades the plant cell and releases its own genetic

material (RNA or DNA) for replication, with increasing levels of viral accumulation depending on the order of viral invasion. Simultaneously, the virus hijacks the host's protein synthesis system to synthesizes viral proteins in large quantities. Subsequently, the virus moves from initial infection sites in epidermal or phloem cells (for insect-borne viruses) into the sieve elements for long-distance movement. The virus then exits the sieve elements in systemically infected tissues by crossing the bundle sheath (BS), vascular parenchyma, and companion

cells (Seo and Kim, 2016; Xue et al., 2023). As the virus moves systemically, it can replicate and/or assemble in many cells to efficiently establish systemic infection. Since virus-induced changes in plant gene expression during the early stages of systemic infection (before symptoms manifest) are key drivers of pathogenesis, understanding these alterations and their roles in viral infection is critical for developing novel virus control strategies.

Maize (*Zea mays* L.), one of the most productive and widely cultivated crops globally, plays an increasingly important role in food production (Pechanova and Pechan, 2015). Maize production is threatened by both abiotic and biotic stresses, including viral infections. Sugarcane mosaic virus (SCMV) is a prevalent monocot-infecting potyvirus that causes maize dwarf mosaic disease (MDMD) in many maize-producing regions of China, Europe, and Africa (Jiang and Zhou, 2002; Fan et al., 2003; Mahuku et al., 2015; Redinbaugh and Stewart, 2018; Braidwood et al., 2019). Over the past several decades, intensive efforts have explored potential measures for controlling SCMV and MDMD (Kannan et al., 2018). However, the molecular events that are crucial to the infection process and pathogenicity of SCMV in maize remain largely elusive.

Recently, we characterized the manifestation of mosaic symptoms following systemic SCMV infection in maize (Jiang et al., 2023). During its distal movement, SCMV travels upward through the vascular system, with mosaic symptoms first appearing at the base of upper leaves (Du et al., 2020; Jiang et al., 2023). The virus then continues to spread, and symptoms emerge in most regions of systemically infected leaves. Consequently, during early systemic infection—before symptoms are visible—the virus enters new cells and begins to multiply, with viral accumulation levels varying widely from absent to high concentrations within different cells of the same leaf. This dynamic process of early systemic SCMV infection in maize provides a suitable study system to explore the patterns of co-variation between viral accumulation and changes in host gene expression at the single-cell level.

Previous omics studies analyzing tissues, organs, or entire organisms, treated samples as homogeneous bulk material, averaging out any variation present among cells within them. The recent development of single-cell RNA sequencing (scRNA-seq) technology makes it possible to resolve cell-to-cell transcriptomic heterogeneity and has been applied to numerous plant species (e.g., *Arabidopsis*, maize, rice, tomato, and cotton; reviewed in Cuperus, 2022; Ryu et al., 2021; Seyffert et al., 2021), providing new perspectives on gene expression and cell-type evolution in plants. Single-cell characterization of gene expression has been performed on multiple tissues in maize, including leaves (Bezrutczyk et al., 2021; Sun et al., 2022; Tao et al., 2022), shoot apical meristems (Satterlee et al., 2020), roots (Ortiz-Ramirez et al., 2021; Li et al., 2022; Cao et al., 2023; Guillotin et al., 2023), anthers (Nelms and Walbot, 2019; Zhang et al., 2021; Washburn et al., 2023), ears (Xu et al., 2021), and seedlings (Marand et al., 2021), providing valuable references for this study.

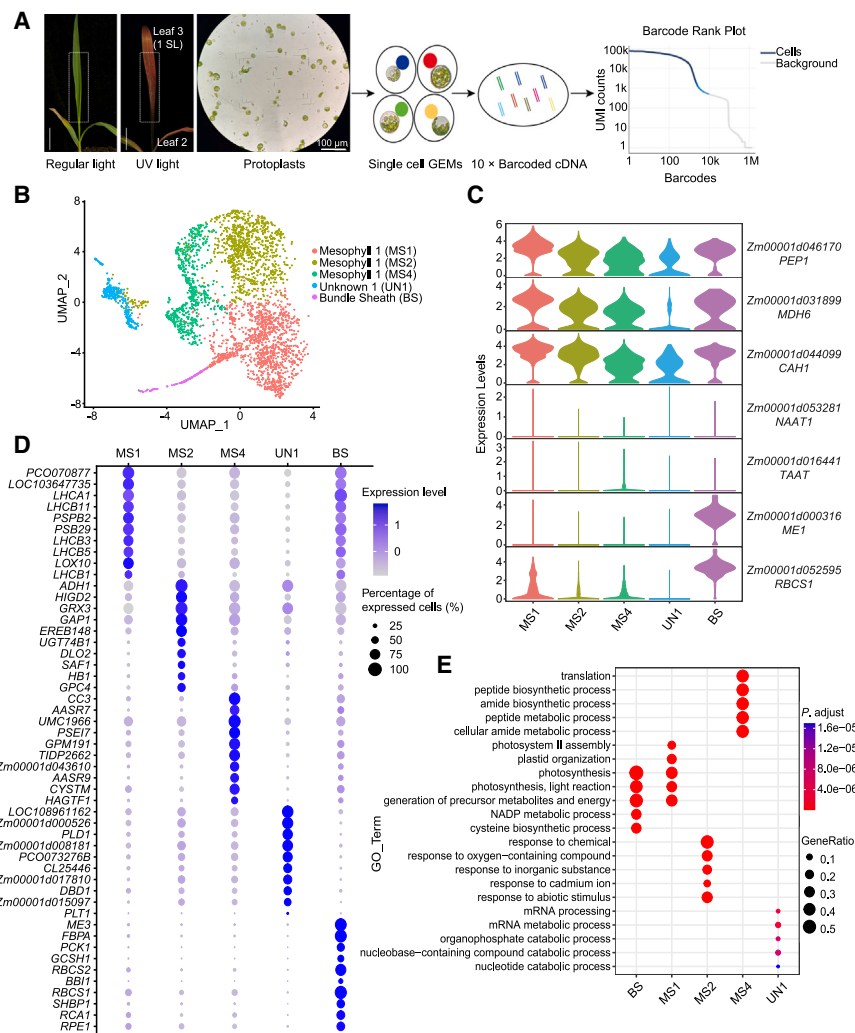
Additionally, scRNA-seq serves as a powerful tool for elucidating the cellular responses of various organisms to a wide array of bi-

## Maize genes altered by viral early systemic infection

otic and abiotic stress conditions. Several studies have applied scRNA-seq to investigate plant responses to biotic stresses. For example, scRNA-seq was used to document the gene expression landscape and identify the molecular features in woodland strawberry leaves at three stages of *Botrytis cinerea* infection (Bai et al., 2022). Liang et al. (2023) investigated the response of rubber leaves to *Oidium heveae* infection by comparing single-cell expression profiles between the control and treated subgroups. Cao et al. (2023) reported single-cell transcriptomes derived from root tips of two maize inbred lines to understand the defense mechanisms of maize roots against *Fusarium verticillioides* infection. Zhu et al. (2023b) utilized scRNA-seq to analyze *Arabidopsis* exposed to *Pseudomonas syringae* to study transcriptional responses ranging from immunity to susceptibility in cell clusters. Yue et al. (2024) described the specific gene expression of each cell type during the infection of tomato chlorosis virus by scRNA-seq. Song et al. (2024) analyzed differentially expressed genes (DEGs) caused by soybean mosaic virus and investigated the antiviral function of soybean glutathione S-transferase proteins. Interestingly, Delannoy et al. (2023) performed three independent scRNA-seq replicates of *P. syringae*-infected *Arabidopsis* leaves without mock conditions, describing the characteristic defense responses of each cell type, with comparative analyses performed with non-challenged *Arabidopsis* plants of the same age (Kim et al., 2021). According to these reports, recent studies further validated the results of bulk RNA-seq by comparing healthy and infected samples, but have not fully exploited the potential of scRNA-seq. Consequently, scRNA-seq still holds great potential in revealing the interactions between plants and viruses.

SCMV is a member of the Potyvirus genus (family Potyviridae) that possesses a positive-sense, single-stranded RNA (+ssRNA) genome with a polyadenylated 3'-terminus (Kannan et al., 2020). These features allow SCMV to be detectable through scRNA-seq, which captures both viral and host messenger RNAs (mRNAs), within infected cells. This principle was demonstrated in a recent report on an animal virus, where scRNA-seq could subsample cells with different viral loads within one sample to analyze molecular distinctions between cells and provide a more detailed view of the host cellular response mechanisms to viruses (Zheng et al., 2022).

In this study, we constructed a single-cell transcriptional landscape of maize leaves during the early stages of systemic infection with SCMV, before the manifestation of symptoms. Given that viral loads vary greatly among individual cells during these early stages, from absent to high concentrations, analyzing the alterations in gene expression levels of each cell in response to the virus will provide key information for determining viral pathogenicity and host susceptibility. Since mesophyll cells serve as both the major replication sites for SCMV and the key cell type displaying mosaic symptoms, we selected mesophyll cells with the highest viral infection rates for in-depth study. Our findings revealed substantial upregulation of host gene expression patterns during the early stages of SCMV systemic infection. Furthermore, we characterized a large number of DEGs and investigated the complex expression patterns between viral accumulation levels and alterations in maize gene expression in infected cells. Moreover, we functionally characterized three pro-viral factors and one anti-viral factor modulating early systemic infection. This



study advances our understanding of the trajectories of SCMV-infected cells as the host plant continues to develop and provides new insights into plant cellular heterogeneity during interactions with viruses at the early stages of systemic infection.

## RESULTS

### The single-cell transcriptome landscape of maize leaves during early systemic infection with SCMV

Given the varying levels of viral accumulation in individual cells of maize leaves during early systemic infection from absent to high levels of viral progeny, we designed a unique sampling method for collecting only SCMV-infected leaf cells but not healthy cells. We selected the early systemic infection stage at 2 h on 5 days post-inoculation (dpi) based on a previous study (Jiang et al., 2023). At this stage, the first systemically infected leaf (referred to as 1 SL) is presymptomatic, whereas some cells of this leaf already exhibit GFP fluorescence, indicating high viral accumulation levels (Figure 1A). The basal portion (0–4 cm) of twenty 1 SLs were harvested (0–4 cm) from SCMV-infected plants and were immediately subjected to protoplast preparation and scRNA-seq (Figure 1A). This unique design employs virus-free cells, termed bystander cells

**Figure 1. Single-cell profiling of SCMV-infected maize leaves during early systemic infection (prior to symptom manifestation).**

(A) Workflow of sampling, single-cell library preparation (including illustrations of protoplast isolation), 10 × chromium gel bead-in-emulsion (GEM) partitioning, cDNA synthesis, RNA sequencing, and data analysis. The second leaves (leaf 2) of maize plants were mechanically inoculated with SCMV-GFP. Protoplasts were isolated from the basal regions (dashed line box) of the third leaves (leaf 3), the first systemically infected leaves (referred to as 1 SLs).

(B) UMAP plots showing a two-dimensional representation of the filtered cells. Cells were grouped into five types. Each dot indicates a single cell, with colors indicating the corresponding cell types.

(C) Violin plots showing the distribution of marker genes across cells in each cluster. These genes are known to be differentially expressed in MS and BS cells in C4 maize.

(D) Dot plots showing expression levels of the top 10 cluster-enriched genes for each cell type. Dot color and size indicate gene expression level and the percentage of cells in which this gene is expressed, respectively.

(E) Dot plots showing overrepresented GO terms among enriched genes in each of the five types. Dot color intensity corresponds to the adjusted p-value (p-value adjusted by the false discovery rate in MAST), and dot size corresponds to the proportion of genes related to a GO term expressed in a type.

in this study, as a healthy control, thereby eliminating the variations observed between infected and healthy plants in traditional designs.

After filtering out low-quality cells, the remaining cells were retained for subsequent analyses. Using uniform manifold approximation and projection (UMAP), nonlinear dimensionality reduction, and unsupervised cell clustering, all cells were divided into five cell types. Reported marker genes in maize were used to annotate these cell types: BS, mesophyll-1 (MS1), MS2, MS4, and a cluster of unknown identity (UN1) that was temporarily classified as a mesophyll cell population (Figure 1B) (Bezrutczyk et al., 2021; Sun et al., 2022; Tao et al., 2022). The marker genes were recognized as DEGs to distinguish MS cells from BS cells in maize (Figure 1C), whose expression patterns within each cell type were consistent with the functional roles of MS and BS cells in C4 photosynthesis (Gao et al., 2022). Subsequently, we analyzed the distribution of the top 10 cluster-enriched genes within each cell type and found distinct cell-type-specific signatures (Figure 1D; Supplemental Table 1).

To further clarify the biological functions of each cell type, we performed Gene Ontology (GO) term enrichment analyses on transcripts expressed in the five cell types (Supplemental

**Table 1**). Each cell type showed distinct over representation of biological processes among expressed genes (Figure 1E; *Supplemental Table 1*). BS was enriched for processes related to photosynthesis (GO:0015979, GO:0019684), generation of precursor metabolites and energy (GO:0006091), NADP metabolism (GO:0006739), and cysteine biosynthesis (GO:0006534). MS1, which accounted for the largest proportion of mesophyll cells, showed enrichment for photosynthesis-related processes (GO:0015979, GO:0019684, GO:0010207), generation of precursor metabolites and energy (GO:0006091), and plastid organization (GO:0009657). MS2 was enriched for responses to abiotic stimuli, including chemicals (GO:0042221), oxygen-containing compounds (GO:1901700), inorganic substances (GO:0010035), and cadmium ions (GO:0046686). MS4 showed expression signatures related to translation (GO:0006412), peptide and amide biosynthetic processes (GO:0043043, GO:0043604), as well as peptide and amide metabolic processes (GO:0006518, GO:0043603). UN1 primarily exhibited activity in mRNA-related processes (GO:0016071, GO:0006397) and nucleotide catabolic processes (GO:0046434, GO:0034655, GO:0009166, GO:0009261, GO:1901292). Results from the Kyoto Encyclopedia of Genes and Genomes (KEGG) pathway enrichment analysis are shown in *Supplemental Table 1*. We detected transcriptional differences among the five cell types, suggesting that these cell subtypes have distinct functions and could provide alternative environments for viral replication and propagation.

#### Identification of virus-free (bystander) and SCMV-infected cells

SCMV has a polyadenylated +ssRNA genome, which allows individual SCMV-infected cells to be identified by aligning scRNA-seq reads to this distinctive viral transcript. The elevated abundance of reads aligning to the 3' UTR is attributed to the poly(A) tail at the 3' terminus of the viral RNA, which enhances binding to poly(dT)VN oligonucleotides on the barcode and facilitates the accurate detection of SCMV-infected cells (Figure 2A). Unexpectedly, viral unique molecular identifiers (UMIs) were detected in nearly every cell of the SCMV-infected sample, with MS4 cells showing the highest viral accumulation levels (Figure 2B). There are two possible explanations for detecting viral reads in a cell: either the virus had previously entered the cell, where virus multiplication generated viral mRNA, or ambient viral mRNA molecules originating from other cells in the same batch contaminated the cell during sampling (Bost et al., 2020; Kotliar et al., 2020). Droplets containing only beads with no cells were used as a background control to exclude ambient viral RNA contamination (see procedures in Materials and Methods). Considering that the threshold of 34 UMIs can eliminate 95% of background interference by ambient viral RNA, we defined a cell as genuinely infected with SCMV if a minimum of 34 viral UMIs were detected (Figure 2C). Cells that did not meet this threshold were defined as bystander cells.

Consistent with the above results, filtering out ambient viral RNAs at single-cell resolution showed that MS4 had the largest proportion of bona fide infected cells and therefore the lowest proportion of bystander cells, whereas UN1 showed the opposite pattern (Figure 2D; *Supplemental Table 2*). Given that mesophyll cells serve as the primary cellular site for SCMV

#### Maize genes altered by viral early systemic infection

replication (Xie et al., 2024), we focused subsequent analyses on these cells, especially MS4 cells, which exhibit an extremely wide range of viral accumulation levels and thus provide an excellent study system.

To clarify the localization of MS4 cells in maize leaf tissue, we selected two MS4-specific marker genes, *ZmGSTU6* and *ZmELFG1*. These two genes exhibited relatively high basal expression levels in maize leaves, and their expression levels in MS4 were significantly higher than those in other cell types (*Supplemental Table 1*). Both of these conditions are important for selecting marker genes, otherwise it is difficult to observe significant differences within *in situ* hybridization assays. *ZmGSTU6* and *ZmELFG1* showed the highest expression levels in MS4 cells on the UMAP plots (Figure 2E). The mRNAs of *ZmGSTU6* and *ZmELFG1* were found predominantly in MS cells adjacent to BS cells, in both SCMV-infected and mock-inoculated leaves (Figure 2F). Interestingly, the localization of the SCMV coat protein (CP) gene largely coincided with that of *ZmGSTU6* and *ZmELFG1* in SCMV-infected leaves (Figure 2F). No staining was visible after hybridization with the sense probes for the corresponding genes (Figure 2F). These results are consistent with the conclusion that MS4 cells have the highest viral accumulation levels (Figure 2B and 2C).

#### Analysis of differential gene expression between infected and bystander cells across four cell types

To investigate transcript level changes in the cells of SCMV-infected samples, we compared gene expression patterns between the infected and bystander cells within each of the four mesophyll cell types. Compared with their corresponding bystander cells, most maize genes were upregulated, whereas few genes were downregulated in the infected cells of each type (Figure 3A; *Supplemental Table 3*). Many significantly upregulated genes in infected cells are involved in translation (GO:0006412), ribosome assembly (GO:0042255, GO:0042256), and ribosome biogenesis (GO:0042254, GO:0022613), as well as in the biosynthetic and metabolic processes of peptide, amide, and organonitrogen compounds (GO:0043043, GO:0006518, GO:0043604, GO:0043603, GO:1901566, GO:1901564) (Figure 3B; *Supplemental Table 3*).

We found that corn cystatin 7 (CC7, *Zm00001d029628*) was upregulated in the infected cells of the MS1, MS2, and MS4 clusters (Figure 3C; *Supplemental Table 4*). CC7 encodes a protein that is homologous to the corn cystatin 9 (CC9) protein, which inhibits apoplastic papain-like cysteine proteases and salicylic acid signaling, including the expression of pathogenesis-related genes, during *Ustilago maydis* infection (van der Linde et al., 2012). The expression level of 40S ribosomal protein S28 (*Zm00001d028807*) was upregulated after infection in MS2, MS4, and UN1 cells, whereas *orf99-d* (*ZeamMp050*) was upregulated in infected MS1, MS2, and UN1 cells (Figure 3C; *Supplemental Table 4*). Two genes (abscisic acid stress ripening 1, ASR1, *Zm00001d023529*; temperature-induced lipocalin 1, *TIL1*, *Zm00001d017199*) were upregulated in infected MS1 and MS2 cells (Figure 3C; *Supplemental Table 4*). ASR1 is known to respond to abscisic acid and multiple abiotic stresses, such as drought, salinity, and metal stress (Virlouvet et al., 2011; Zhang

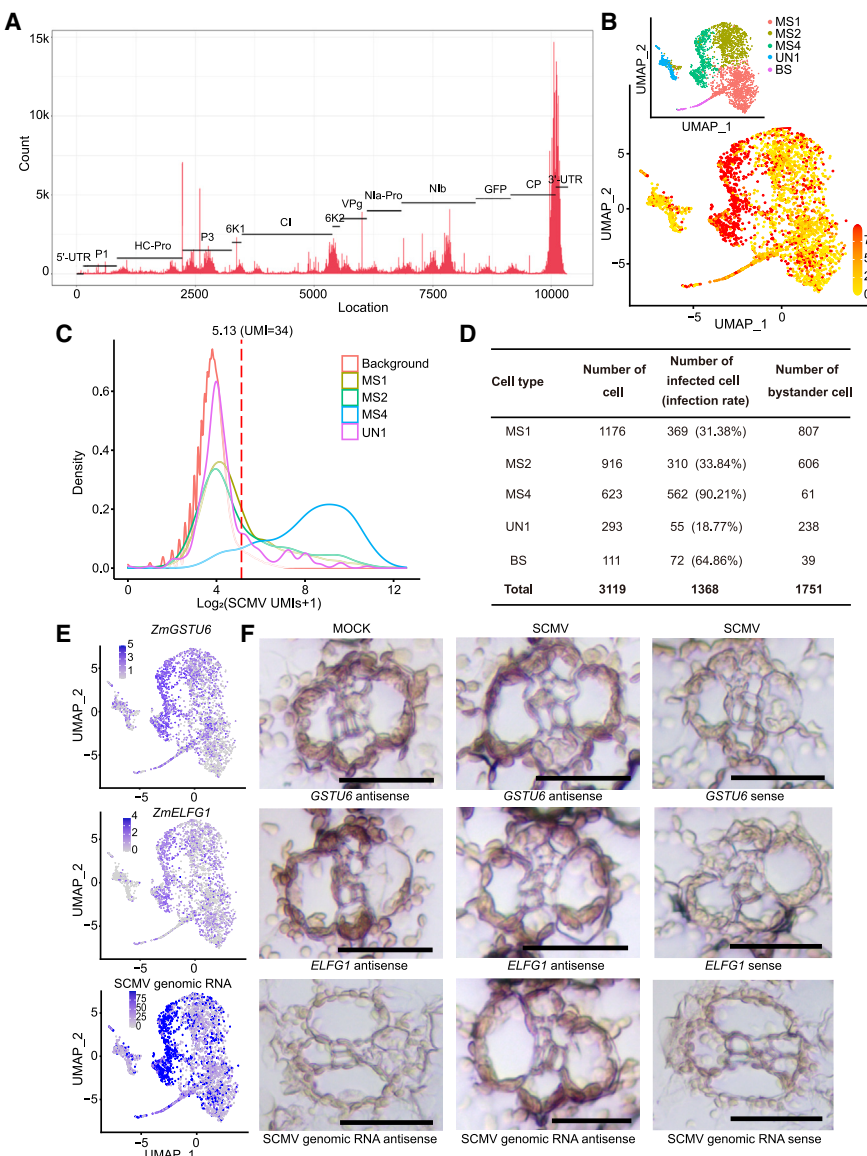


**Figure 2. Virus distribution and identification of virus-free (bystander) and SCMV-infected cells.**

(A) Histogram showing the alignment of reads obtained by scRNA-seq to the SCMV genome. The abscissa corresponds to the SCMV genome sequence, and the ordinate represents the abundance of viral genome alignment in each region.

(B) UMAP plots showing viral accumulation levels in each single cell. Darker colors represent higher viral accumulation levels.

(C) Density distribution decays showing the distribution of viral loads across the four cell types. The abscissa values represent SCMV UMIs after log transformation, and the area between each curve and the X-axis is 1. Colors represent the corresponding cell types. Background UMIs result from ambient SCMV RNA contamination. The dashed line indicates a threshold of 34 after log transformation.

(D) Presentation of cell numbers and infection rates for each of the five cell types. Cells with viral UMI counts greater than 34 were defined as infected cells, and those with counts lower than 34 as bystander cells.

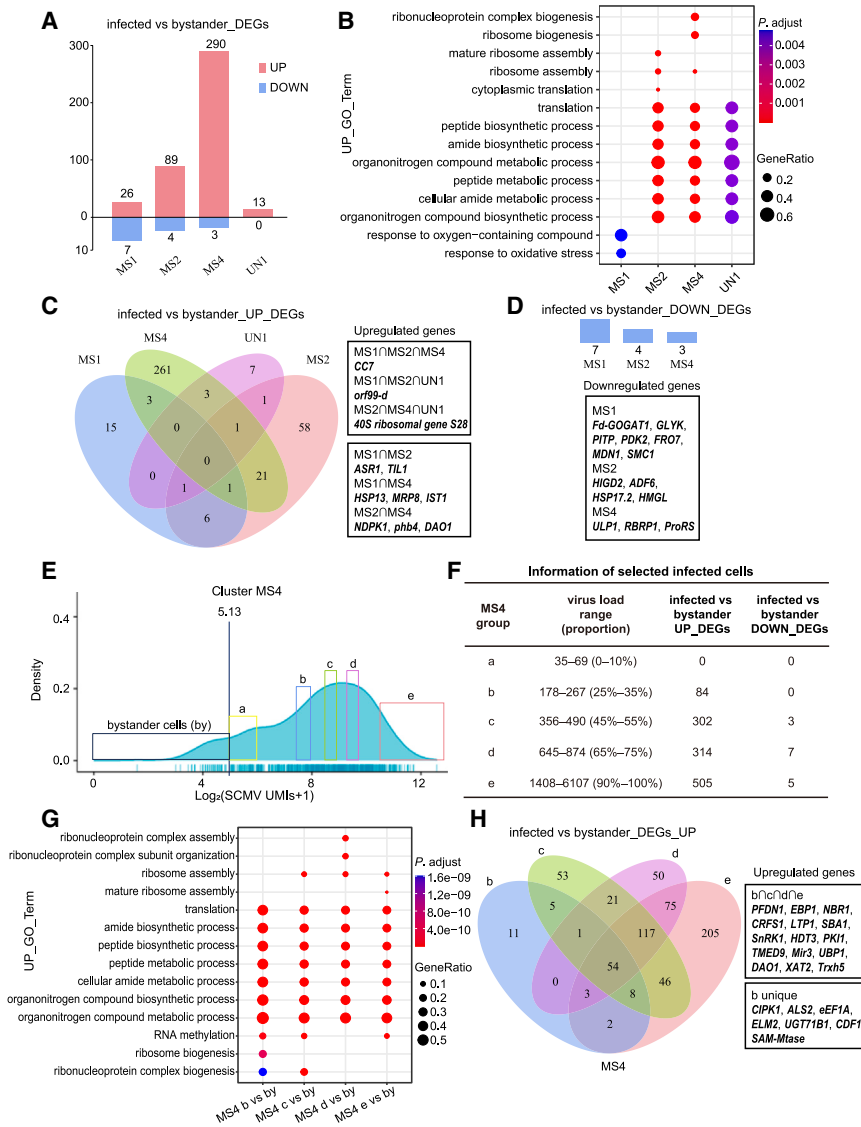
(E) UMAP projection plots showing transcript accumulation levels of *GSTU6*, *ELFG1*, and SCMV genomic RNA at single-cell resolution. The color intensity represents the relative transcript expression level for the indicated gene in each cell.

(F) RNA *in situ* hybridization using antisense and sense probes for *GSTU6*, *ELFG1*, and SCMV CP genes in SCMV-infected and mock-inoculated leaf tissue. Scale bars correspond to 100  $\mu$ m.

et al., 2019), and *TIL1* is involved in tolerance to temperature, oxidative, salt, drought, and high light stress (Frenette Charron et al., 2002; Chi et al., 2009; Abo-Ogiala et al., 2014; He et al., 2015).

Three genes were upregulated in infected MS1 and MS4 cells: *heat shock protein 13* (*HSP13*, *Zm00001d052855*), *multidrug*

*resistance-associated protein 8* (*MRP8*, *Zm00001d008733*), and *increased salt tolerance 1* (*IST1*, *Zm00001d024425*) (Figure 3C; Supplemental Table 4). *IST1* plays a vital role in regulating the activity of the AAA-type ATPase Vps4, which executes the disassembly of ESCRT-III, an essential step in multivesicular body vesicle formation (Dimaano et al., 2008; Buono et al., 2016). Both MS2 and MS4 cells showed upregulation of three genes



following SCMV infection: nucleoside diphosphate kinase 1 (*NDPK1*, *Zm00001d029968*), prohibitin 4 (*phb4*, *Zm00001d034795*), and dioxygenase for auxin oxidation 1 (*DAO1*, *Zm00001d003311*) (Figure 3C; Supplemental Table 4). *NDPK1* belongs to type I *NDPKs*, which are involved in metabolism, growth, development, and stress responses (Dorion and Rivoal, 2015). *NDPKs* have been reported to upregulate in response to drought, abscisic acid, heat, and salinity (Salekdeh et al., 2002; Cho et al., 2004; Hajheidari et al., 2005; Dooki et al., 2006; Lee et al., 2007).

Unlike the upregulated genes, all genes that were downregulated in response to viral infection were unique to individual cell types (Supplemental Table 3). For example, *ferredoxin-dependent glutamate synthase 1* (*Fd-GOGAT1*, *Zm00001d022388*), *D-glycerate-3-kinase* (*GLYK*, *Zm00001d035737*), *pyruvate dehydrogenase kinase 2* (*PDK2*, *Zm00001d022274*), and *ferric reduction oxidase 7* (*FRO7*, *Zm00001d003559*) were downregulated in MS1 cells; *hypoxia-induced protein 2* (*HIGD2*, *Zm00001d017060*), *actin depolymerizing factor*

**Figure 3. Analysis of DEGs between infected and bystander cells within the four cell types as well as distinct viral accumulation levels in MS4.**

(A) Histogram showing the number of DEGs between infected and bystander cells within four cell types. Red columns represent upregulated DEGs and blue columns represent downregulated DEGs.

(B) Dot plots showing enriched GO terms among upregulated DEGs between infected and bystander cells across the four cell types. Dot color intensities correspond to adjusted *p*-values (*p*-value adjusted by the false discovery rate in MAST), and dot sizes correspond to the proportion of genes related to each GO term that are expressed in a cell type.

(C) Venn diagram depicting overlapping upregulated DEGs among the four cell types for infected cells compared with bystander cells.

(D) Histogram showing downregulated DEGs between three cell types for infected cells compared with bystander cells.

(E) Density distribution decay showing the distribution of viral loads in MS4. Sections labeled "a, b, c, d, and e" represent cells within different viral accumulation level intervals in MS4.

(F) Table showing information about the infected cells in intervals "a, b, c, d, and e" within MS4.

(G) Dot plots showing enriched GO terms among upregulated DEGs between infected cells with distinct viral accumulation levels (i.e., b, c, d, and e) and bystander cells in MS4.

(H) Venn diagram showing overlapping upregulated DEGs between infected cells with distinct viral accumulation levels (i.e., b, c, d, and e) and bystander cells in MS4.

in MS2 cells, *HMGL* (*Zm00001d052444*) was downregulated and *prolyl-tRNA synthetase* (*PRS*, *Zm00001d053196*) was downregulated in MS4 cells (Figure 3D; Supplemental Table 3).

Taken together, SCMV infection primarily caused the upregulation of maize genes, and only a small number of genes were downregulated. In addition to upregulating translation-related and other virus-susceptibility genes, SCMV infection also upregulated many genes involved in stress resistance. Although few genes were downregulated, it is noteworthy that they are associated with stress responses. Based on these results, we identified candidate genes that may contribute to conditioning SCMV systemic infection.

#### Differences in the transcriptomes of bystander cells and infected cells with distinct viral accumulation levels in MS4

To focus on the molecular differences between cells under different viral replication states, we subsampled MS4 cells according to their viral accumulation levels (Figure 3E). As

## Maize genes altered by viral early systemic infection

intracellular viral accumulation levels increased in MS4 cells, the number of DEGs between infected and bystander cells also increased significantly (Figure 3F; Supplemental Table 5). GO analyses of DEGs between bystander and infected cells under different viral replication states showed enrichment of similar biological processes (Figure 3G; Supplemental Table 5). DEGs significantly upregulated in infected cells are involved in translation (GO:0006412), ribosome assembly (GO:0042255), and RNA methylation (GO:0001510), as well as in the biosynthetic and metabolic processes of peptides, amides, and organonitrogen compounds (GO:0043043, GO:0006518, GO:0043604, GO:0043603, GO:1901566, GO:1901564).

Moreover, the majority of DEGs were shared among infected cells under different viral replication states, including *neighbor of BRCA1* (NBR1, Zm00001d017072), *non-specific lipid transfer proteins 1* (nsLTP1, Zm00001d029365), *maize insect resistance 3* (Mir3, Zm00001d002065), *thioredoxin h-type 5* (Trxh5, Zm00001d034491), and *DAO1* (Zm00001d003311) (Figure 3H; Supplemental Table 5).

In addition, we identified genes that rapidly respond to SCMV infection at low viral accumulation levels (i.e., DEGs only present in the “b” vs. bystander group) (Figure 3H). These genes include *CBL-interacting protein kinase 1* (CIPK1, Zm00001d040567), *acetolactate synthase 2* (ALS2, Zm00001d016572), *elongation factor 1-alpha* (eEF1A, Zm00001d037877), *elongated mesocotyl 2* (ELM2, Zm00001d046492), *UDP-glycosyltransferase 71B1* (UGT71B1, Zm00001d021571), *cell growth defect factor 1* (CDF1, Zm00001d020344), and *S-adenosyl-L-methionine-dependent methyltransferase* (SAM-Mtase, Zm00001d003276).

## Dynamically co-varying expression patterns of maize genes in relation to viral accumulation levels in infected cells

To investigate the relationship between gene expression patterns and viral accumulation levels, we grouped maize genes expressed in MS4 cells into ten modules based on their expression values (Figure 4; Supplemental Table 7) using the Mfuzz package (Kumar and Futschik, 2007; Wang et al., 2016a). Gene expression levels in modules A to E increased significantly at specific stages corresponding to changes in viral accumulation levels but remained relatively constant at other stages. Expression levels of genes in modules F to I generally showed an upward trend, whereas those in module J slightly decreased during phases that exhibited high viral accumulation levels. Module I contained the largest number of genes, while modules A to D harbored fewer genes (Figure 4; Supplemental Table 7).

Next, we performed KEGG pathway enrichment analyses on genes in different Mfuzz modules (Figure 4; Supplemental Table 8). Several pathways known to play roles in viral infection were enriched, such as carbon metabolism (modules G, H, and I), citrate cycle (modules G and H), and oxidative phosphorylation (modules G, H, and I), all of which are capable of providing energy for viral propagation (Polcicova et al., 2020). Similarly, as viral accumulation levels increased, the expression levels of genes regulating ribosome activity (modules G and I) and amino acid biosynthesis (modules G and

## Plant Communications

I) also increased, effectively sustaining viral protein synthesis (Ohlson et al., 2023).

During viral infection, plants may employ resistance mechanisms to combat infection, which can also be exploited by viruses. For instance, ubiquitin-mediated proteolysis (modules F, G, and I), proteasome activity (modules G and I), and autophagy (modules E and H) are commonly involved in resistance responses (Dielen et al., 2010; Yang et al., 2020; Lobaina et al., 2022). Additionally, peroxisome activity (modules F and I) (Laliberté and Sanfaçon, 2010), spliceosome activity (modules G, H, and I) (Meyer, 2016), endocytosis (modules E and G) (Wu et al., 2018; Wu et al., 2020), glutathione metabolism (modules G and I) (Höller et al., 2010), sulfur metabolism (module J) (Gao et al., 2012), fatty acid degradation (modules H and I) (Wang et al., 2024), and SNARE interactions in vesicular transport (module G) (Cabanillas et al., 2018) have been implicated in viral infections. Interestingly, the co-expression patterns of multiple genes within the same pathway varied in response to viral accumulation levels, indicating a diverse range of responses to viral infection within individual pathways (Figure 4; Supplemental Table 8).

Expression patterns of genes that co-varied with elevated viral accumulation levels in MS1 and MS2 cells, grouped into Mfuzz modules, are presented in Supplemental Figures 1A and 1B and Supplemental Table 7. In summary, the expression levels of maize genes associated with either resistance or susceptibility to SCMV predominantly increased in response to elevated viral accumulation levels.

## Reconstruction of developmental trajectories for SCMV-infected maize cells

One key advantage of scRNA-seq is its ability to leverage gene expression profiles of individual cells to reconstruct the developmental trajectories that shape cell populations. To assess the continuous differentiation trajectories of individual cells in our SCMV-infected sample, we inferred a pseudotime trajectory using R packages Monocle 2 and CytoTRACE. The results indicated that the pseudotime trajectory had two branch points, which divided the cell population into one of five states (Figure 5A and 5B and Supplemental Figure 2A). Cells shifted gradually from state 5 to state 1 or 4 (Figure 5B), indicating that the differentiation trajectory started with MS4 cells transitioning into MS2 cells, and then branched into either MS1 or UN1 cells (Figure 5C).

To confirm these patterns, we used CytoTRACE to determine the predicted order of cell differentiation based on developmental potential, from most mature (lowest values) to most immature (highest values) (Gulati et al., 2020). As expected, CytoTRACE predicted that MS4 cells had the highest developmental potential, followed by MS2 and MS1 cells, whereas UN1 cells were the most mature (Figure 5D and 5E).

Following this, we performed RNA velocity analysis, which estimates the rate of expression changes of individual genes at given time points by analyzing the ratios of its spliced (mature) and unspliced (native) mRNA (La Manno et al., 2018; Bergen et al., 2020, 2021). We exported UMAP-based embeddings from Seurat to plot individual cell velocities and vector fields and used

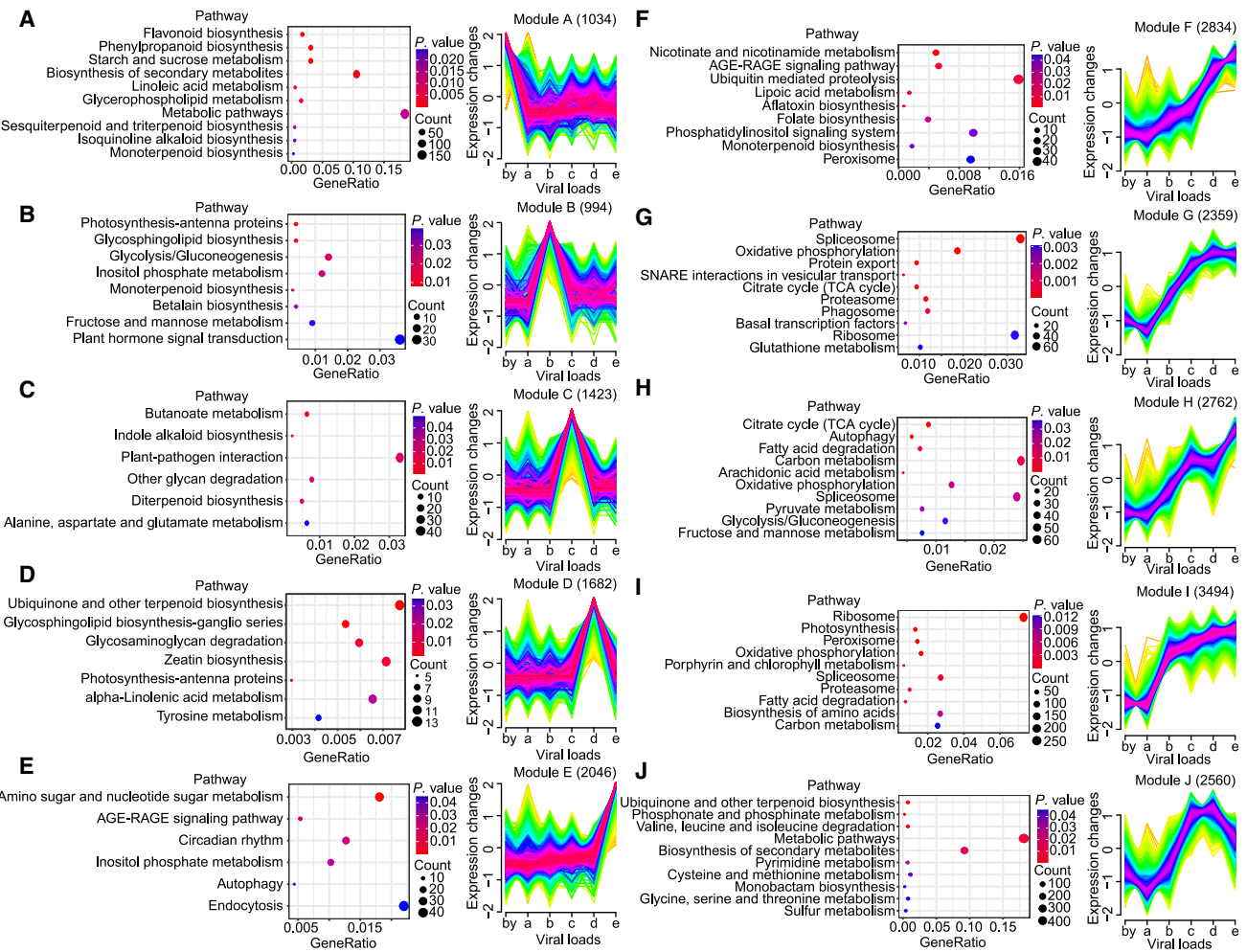


**Figure 4. Transcriptomic characteristics of infected cells with elevated viral accumulation levels in MS4 cells.**

(A–J) Line plots on the right show Mfuzz modules derived from the expression patterns of maize genes in relation to variation in viral accumulation levels among MS4 cells. A total of 10 modules were identified based on these expression patterns. Yellow or green lines indicate genes with low membership values, while red and purple lines correspond to genes with high membership values. The abscissa values represent the viral accumulation levels, and the letters a, b, c, d, and e correspond to the degrees of viral accumulation as shown in Figure 3E. Dot plots on the left show enriched KEGG pathways among maize genes in these 10 Mfuzz modules. Dot color intensities correspond to *p*-values, and dot sizes indicate the counts of genes from each enriched KEGG pathway that are expressed in infected cells.

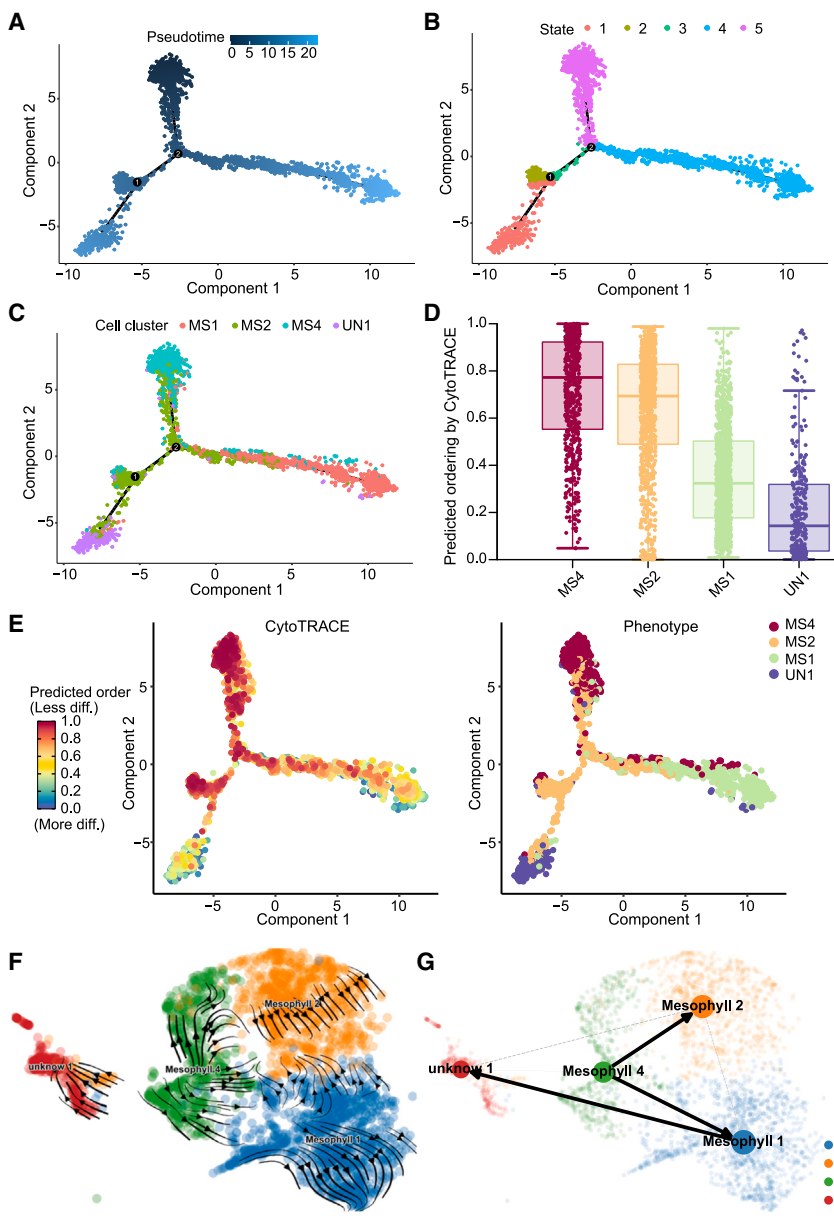
directed-partition-based graph abstraction to visualize the main lineage and developmental trends (Wolf et al., 2019). The results recapitulated the main developmental trends we identified above: MS4 cells initially differentiate into the intermediate MS2 and MS1 states, which then form cells of the terminal cluster UN1 (Figure 5F and 5G).

Taken together, by employing these methodologies, we successfully reconstructed the developmental trajectories of cells in SCMV-infected maize leaves. However, experimental validation through lineage tracing will be required to confirm the directionality of our proposed trajectory.

#### Functional analysis of potential anti- or pro-viral factors during SCMV infection

Based on previous studies (Jiang et al., 2022; Jiao et al., 2022; Gao et al., 2024; Tian et al., 2024; Xie et al., 2024; Yuan et al.,

2024) and the current scRNA-seq analysis, we summarized and speculated on potential anti- or pro-SCMV factors in maize (Figure 6A). Among the candidate factors, we selected four genes for functional validation: *ZmSAM-Mt*, *ZmCDF1*, *ZmCC7*, and *ZmPLT1*. The expression levels of *ZmSAM-Mt* and *ZmCDF1* were significantly upregulated only at low viral accumulation levels (Figure 3H), whereas *ZmPLT1*, a marker gene for UN1 cells (Figure 1D), was uniquely identifiable from the scRNA-seq data in this study. In addition, *ZmCC7* was upregulated in the infected cells of MS1, MS2, and MS4 compared with bystander cells (Figure 3C). Therefore, we selected these four genes for in-depth analysis. UMAP plots illustrating their expression levels at single-cell resolution revealed that *ZmSAM-Mt* and *ZmCDF1* showed higher expression levels in MS1, MS2, and MS4 cells. *ZmCC7* was predominantly expressed in MS4 cells, whereas *ZmPLT1* exhibited low expression levels across various cell types, with notably high expression only in some UN1 cells (Figure 6B).



We then extracted transcriptome data from whole-leaf transcriptome sequencing data conducted by Jiang et al. (2023) at 2 h on 5 dpi (a pre-symptomatic infection stage). Within this dataset, we compared differential expression between SCMV-infected samples and mock-inoculated controls (Supplemental Table 10). The analysis revealed 426 significantly upregulated and 14 downregulated genes. Notably, *ZmCC7*, a candidate gene identified in this study, was significantly upregulated in bulk RNA-seq data (ranking 123rd among significantly upregulated genes; Log<sub>2</sub>FC = 1.965). However, the expression levels of the other three genes, *ZmPLT1* (Log<sub>2</sub>FC = 0.37), *ZmSAM-Mtase* (Log<sub>2</sub>FC = 0.19), and *ZmCDF1* (Log<sub>2</sub>FC = -0.488) did not change significantly. To analyze their overall transcriptional levels in maize leaves during the early stages of SCMV systemic infection, samples were collected from 1 SLs in SCMV-infected and mock-inoculated leaf tissue at 3, 5, 7, and 9 dpi. The results showed that the expression patterns of these four genes varied significantly in

**Figure 5. Developmental trajectories of four mesophyll cell types.**

(A–C) The order of cells along the differentiation trajectory by pseudotime, branch state, and cell type. Each dot represents a single cell, with different colors indicating different cell types or states.

(D) Boxplots showing CytoTRACE values for the four cell types. CytoTRACE values represent differentiation states. The highest values indicate the most immature state, and the lowest values indicate the most mature state.

(E) Unrooted trees showing complex branching processes during mesophyll differentiation as identified by CytoTRACE. Plots in the left panel are ordered identically by CytoTRACE, while those in the right panel show previously annotated phenotypes.

(F) UMAP plots showing RNA velocity estimates for cells from the four mesophyll types. Streamlines represent the predicted developmental trends, and colors correspond to the respective cell types.

(G) Trajectories between cell types as inferred by Directed-PAGA. The directions of the arrows indicate the predicted developmental trends.

response to SCMV infection compared with mock-inoculated plants (Figure 6C).

To determine the function of the four genes in SCMV infection, we knocked down the expression of *ZmSAM-Mt*, *ZmCDF1*, *ZmCC7*, and *ZmPLT1* individually using a cucumber mosaic virus (CMV)-induced gene silencing vector, as described previously (Wang et al., 2016b). Maize plants inoculated with CMV-GUS served as negative controls. The CMV-inoculated maize seedlings were then challenge-inoculated with SCMV at the two-leaf stage. Silencing of *ZmSAM-Mt*, *ZmCDF1*, *ZmCC7*, or *ZmPLT1* did not affect maize seedling growth (Supplemental Figure 3A). Following SCMV

infection, markedly milder mosaic symptoms were observed in *ZmSAM-Mt*-, *ZmCDF1*-, and *ZmCC7*-silenced plants compared with control plants, while *ZmPLT1*-silenced plants manifested pronounced leaf chlorosis (Figure 7A). Samples were collected for virus detection at 2 h on 5 dpi of SCMV. Reverse-transcription quantitative polymerase chain reaction (RT-qPCR) analysis showed that, the expression level of *ZmSAM-Mt*, *ZmCDF1*, *ZmCC7*, and *ZmPLT1* were reduced by approximately 50% in 1 SLs of silenced plants at 10 dpi (Figure 7B). Meanwhile, SCMV genomic RNA levels were reduced by approximately 50% in 1 SLs of *ZmSAM-Mt*-, *ZmCDF1*-, and *ZmCC7*-silenced plants but increased by about 1.5-fold in *ZmPLT1*-silenced plants compared with controls (Figure 7B). Immunoblot results paralleled these findings (Figure 7C).

To further explore the roles of these genes, we utilized the SCMV-GFP infectious clone to overexpress *ZmSAM-Mt*,

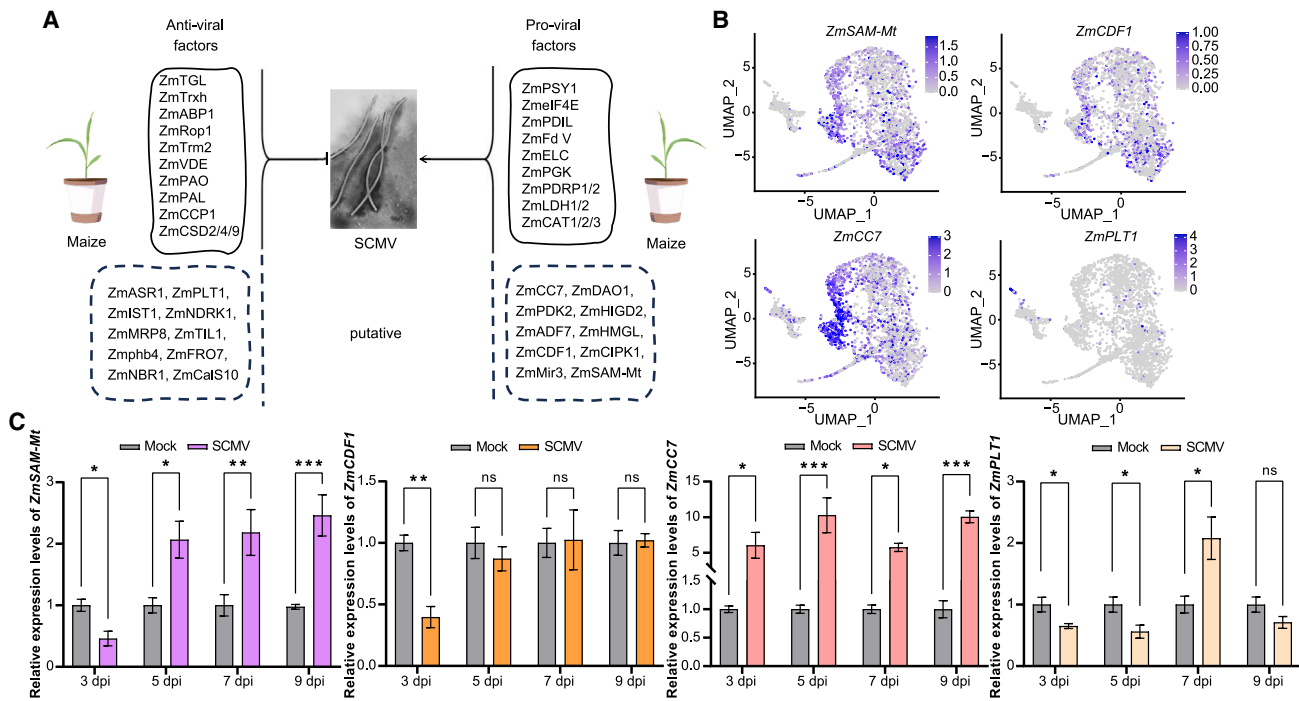


**Figure 6. Putative anti- or pro-viral factors responding to SCMV infection.**

(A) Model depicting molecular interplays between SCMV and maize plants. Reported anti-viral factors (upper-left) and pro-viral factors (upper-right) are listed in solid line boxes. The putative anti-viral factors (lower-left) and pro-viral factors (lower-right) are in dashed boxes.

(B) UMAP projection plots showing transcript accumulation levels of *ZmSAM-Mt*, *ZmCDF1*, *ZmCC7*, and *ZmPLT1* genes at single-cell resolution. Color intensity represents the relative transcript expression level for each indicated gene in each cell.

(C) Transcript levels of *ZmSAM-Mt*, *ZmCDF1*, *ZmCC7*, and *ZmPLT1* genes in maize determined by reverse transcription quantitative PCR (RT-qPCR) at 3, 5, 7, and 9 dpi with SCMV (colored bars). Plants inoculated with phosphate buffer (mock, gray bars) are used as controls. Statistical differences (ns, no significant difference; \*P < 0.05, \*\*P < 0.01, \*\*\*P < 0.001) are evaluated using Student's t-test.

*ZmCDF1*, *ZmCC7*, and *ZmPLT1* separately following the method we recently reported (Xie et al., 2024). The GFP fragment between the N1b and CP cistrons on the pSCMV-GFP vector was replaced with the coding sequence of FLAG-tagged *ZmSAM-Mt*, *ZmCDF1*, *ZmCC7*, or *ZmPLT1* to obtain the reconstructed vectors (Figure 7D), with pSCMV-GFP-FLAG as a control. Overexpression of *ZmSAM-Mt*, *ZmCDF1*, *ZmCC7*, or *ZmPLT1* did not affect maize seedling growth but altered the appearance of mosaic symptoms (Supplemental Figure 3B). Plants infected with SCMV-SAM-Mt-FLAG, SCMV-CDF1-FLAG, and SCMV-CC7-FLAG, exhibited more pronounced mosaic symptoms on 1 SLs compared with the control plants, while SCMV-PLT-FLAG-infected plants showed milder mosaic symptoms (Figure 7E). Virus detection was conducted on samples collected at 2 h on 5 dpi. The accumulation of SCMV genomic RNA and CP increased in SCMV-SAM-Mt-FLAG, SCMV-CDF1-FLAG, and SCMV-CC7-FLAG-infected plants, and decreased in SCMV-PLT-FLAG-infected plants, compared with SCMV-GFP-FLAG-infected plants (Figure 7F and 7G). The protein expression of FLAG-tagged *ZmSAM-Mt*, *ZmCDF1*, *ZmCC7*, *ZmPLT1*, and GFP were also detected through immunoblot (upper panels in Figure 7G). Despite the lower expression levels of *ZmSAM-Mt*, *ZmCDF1*, *ZmCC7*, and *ZmPLT1* proteins compared to GFP, their respective promotional or inhibitory effects on the CP protein were significant (Figure 7G).

Collectively, these results suggest that *ZmSAM-Mt*, *ZmCDF1*, and *ZmCC7* function as susceptibility factors that promote SCMV infection and *ZmPLT1* acts as an antiviral factor that inhibits SCMV infection.

## DISCUSSION

### Selection and analysis of SCMV-infected sample for scRNA-seq

scRNA-seq has become a valuable tool for life science research; however, its application in understanding viral infections in plant hosts remains relatively rare. In this study, we utilized scRNA-seq to analyze altered gene expression and identify maize genes crucial for systemic infection by SCMV. We focused on the early stage of systemic infection (pre-symptomatic infection), as molecular interactions between SCMV and maize at this stage are crucial for determining symptom manifestation and severity. Moreover, since various levels of viral accumulation are observed in different cells of the first systemically infected maize leaf during the early systemic infection stage, our unique design required sampling only SCMV-infected, not healthy, leaves. Coincidentally, Delannoy et al. (2023) collected *Arabidopsis* leaves at 16 h post-inoculation as healthy controls. Because *P. syringae* selectively colonizes plant tissues at this time point, it was assumed that the majority of plant cells would be unaffected. However, their

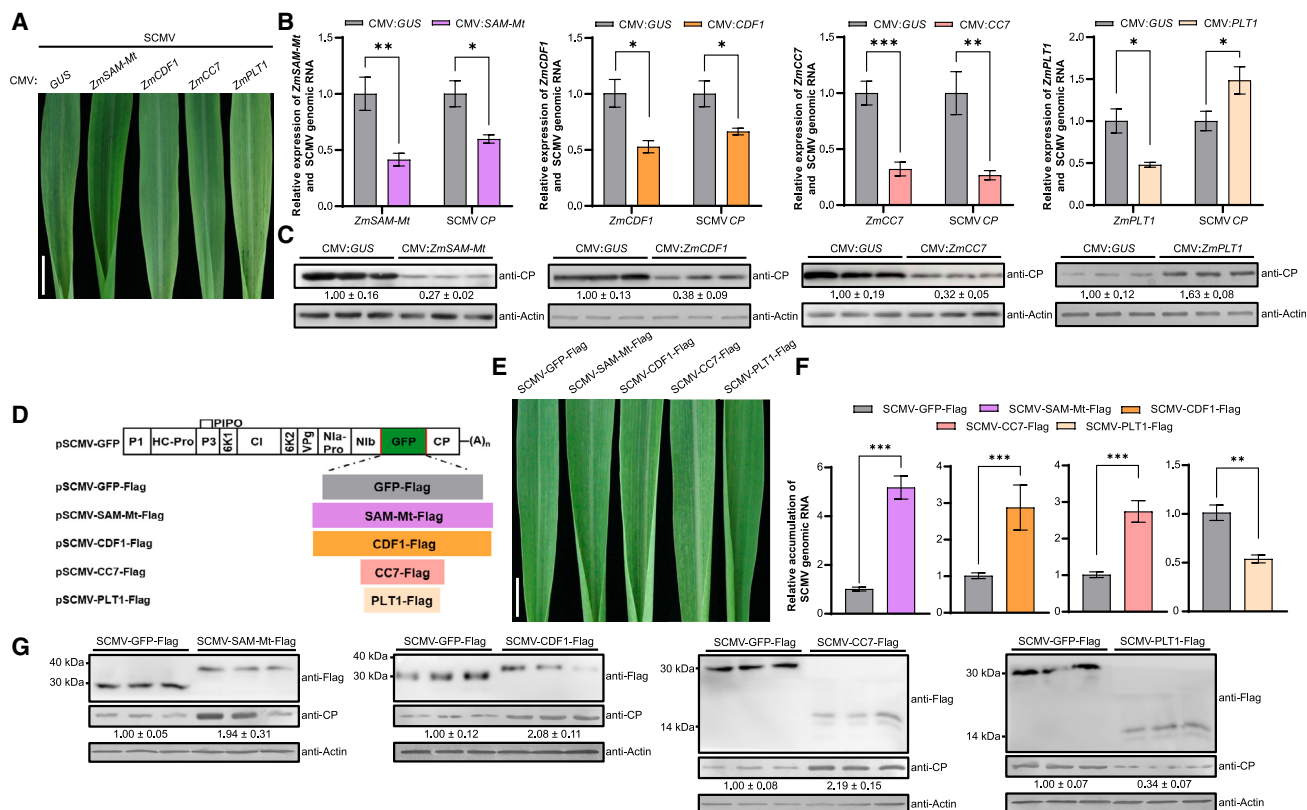


**Figure 7. Systemic SCMV infection by silencing or overexpressing ZmSAM-Mt, ZmCDF1, ZmCC7, and ZmPLT1 in maize.**

(A) Mosaic symptoms on systemically infected leaves caused by silencing ZmSAM-Mt, ZmCDF1, ZmCC7, or ZmPLT1 in maize using CMV-VIGS. Maize plants inoculated with CMV:GUS are used as controls. Scale bars correspond to 1 cm.

(B) RT-qPCR analysis of the relative accumulation levels of ZmSAM-Mt, ZmCDF1, ZmCC7, or ZmPLT1 genes and SCMV genomic RNA in gene-silenced plants. Statistical differences (\*P < 0.05, \*\*P < 0.01, \*\*\*P < 0.001) are evaluated using Student's t-test.

(C) Relative abundance of SCMV CP in gene-silenced plants measured via immunoblotting and visualized using ImageJ software. Actin serves as the loading control. Results are presented as mean ± SE (n = 3).

(D) Schematic organization of recombinant SCMV-related constructs.

(E) Mosaic symptoms on systemically infected leaves caused by overexpression of ZmSAM-Mt, ZmCDF1, ZmCC7, and ZmPLT1 genes in maize using an SCMV infectious clone. Maize plants inoculated with SCMV-GFP-Flag are used as controls. Scale bars correspond to 1 cm.

(F) RT-qPCR analysis of relative accumulation levels of SCMV genomic RNA in gene-overexpressing plants. Statistical differences (\*P < 0.05, \*\*P < 0.01, \*\*\*P < 0.001) are evaluated using Student's t-test.

(G) Detection of GFP-FLAG, SAM-Mt-FLAG, CDF1-FLAG, CC7-FLAG, PLT1-FLAG, and SCMV CP through immunoblotting. Relative abundance of SCMV CP in gene-overexpressing plants is measured via immunoblotting and visualized using ImageJ software. Actin serves as the loading control. Results are presented as mean ± SE (n = 3).

control samples included non-challenged *Arabidopsis* plants of the same age from another study (Kim et al., 2021), resulting in significant individual differences. To take full advantage of scRNA-seq, this study used bystander cells as the healthy control, thereby avoiding the biases between infected and healthy plants observed in traditional designs.

Because SCMV has a single-stranded positive-sense RNA genome with 3' polyadenylation, it is efficiently captured during mRNA isolation using scRNA-seq technology. This has allowed us to explore the patterns of co-variation between viral accumulation levels and changes in gene expression across maize cells. This methodological approach aligns with a previous study that utilized the African swine fever virus, a double-stranded DNA virus. In that study, scRNA-seq was employed to differentiate macrophages infected with varying loads of the virus, enabling the analysis of both host and viral gene

expression profiles. Cells with the highest and lowest top-ranked 10% viral loads were subsampled and molecular differences between these two virus replication states were analyzed (Zheng et al., 2022). In the present study, cells were subdivided into six groups according to viral loads (Figures 3E, 3F, and 4), and we conducted comprehensive, varied, and continuous comparative analyses among these groups.

Immunogold labeling assays, previously conducted to quantify double-stranded RNA, revealed significantly more gold particles in MS than BS cells, indicating that MS cells serve as the major cellular sites for SCMV replication (Xie et al., 2024). Furthermore, the present study focused on MS cells, particularly MS4 cells, which exhibit an extremely wide range of viral accumulation levels and serve as an excellent system for studying SCMV.

## Plant Communications

### Speculation on the mechanism of UN1 cells appearance

Following scRNA-seq, we leveraged known marker genes to categorize cells from SCMV-infected maize leaves into five cell types. Interestingly, an additional cell type, UN1, emerged during the early stages of systemic infection. To clarify the mechanism underlying the appearance of UN1 during viral infection, we first analyzed the expression of marker genes enriched in UN1, such as *proton pump interactor 1* (*PPI1*, *Zm00001d020965*), *phospholipid transfer protein 1* (*PLT1*, *Zm00001d023343*), *multi-drug resistance-associated protein 1* (*MRP1*, *Zm00001d046226*), and *callose synthase 10* (*CalS10*, *Zm00001d030266*) (Supplemental Table 1). Plasma membrane H<sup>+</sup>-ATPases are involved in a variety of physiological processes such as growth and development, and responses to abiotic stress. Moreover, *PPI1* is a novel interactor of the C-terminal autoinhibitory domain of the proton pump and stimulates H<sup>+</sup>-ATPase activity (Anzi et al., 2008). *StPPI1* mRNA levels are induced by salt stress, cold, drought, and mechanical wounding (Muniz Garcia et al., 2011). PLTPs may be involved in membrane biogenesis, intracellular distribution of phospholipids, plant signaling, and defense against phytopathogens (Vergnolle et al., 1992; Carvalho and Gomes, 2007). It was reported that *StLTP6* was significantly upregulated in potato infected with either potato virus Y or potato virus S. *StLTP6* inhibited the expression of several genes in the RNA silencing pathway, thereby promoting viral infection by inhibiting virus-induced RNA silencing (Shang et al., 2022). In another study, *NbLTP1* was induced following infection with tobacco mosaic virus, which could activate pathogenesis-related genes by upregulating salicylic acid biosynthesis to repress viral infection (Zhu et al., 2023a). Furthermore, cowpea LTP1 suppresses the accumulation of cowpea mosaic virus and soybean mosaic virus by directly inhibiting viral cysteine protease activity (Ji et al., 2024). It was postulated that *ZmMRP1* and *ZmMRP2* could transport agents or products of oxidative stress (Swarbreck et al., 2003). TaMRPs respond to *F. graminearum* and enhance wheat resistance to *Fusarium* head blight disease by activating JA (Walter et al., 2015). Callose formation is a defense response that can limit or block viral cell-to-cell movement (Zavaliev et al., 2011), and callose synthase genes are responsible for callose biosynthesis. Callose deposition has been shown to improve plant resistance to bamboo mosaic virus (Alazem et al., 2017), tomato yellow leaf curl virus (Yang et al., 2022), cassava brown streak virus (Anjanappa et al., 2018), and tobacco mosaic virus (Li et al., 2021; Zhong et al., 2021).

In addition, the GO term and KEGG pathway enrichment analyses of UN1 cells suggested that mRNA processing and surveillance were particularly active in this cell type (Figure 1E; Supplemental Table 1). Regulation of mRNA processing and stability is an efficient molecular mechanism that enables cells to maintain translatable transcripts throughout mRNA surveillance. RNA surveillance ensures that only properly processed, mature mRNAs are translated, preventing the generation of abnormal transcripts that may encode mutated or harmful proteins (Wagner and Lykke-Andersen, 2002; Moraes, 2010). Studies suggest that mRNA surveillance mechanisms serve as intrinsic barriers to the translation of early viral proteins and the amplification of +RNA viruses, including sorghum mosaic virus, rice stripe virus, potato virus X, and Semliki

### Maize genes altered by viral early systemic infection

Forest virus (Balistreri et al., 2014; Garcia et al., 2014; Jin et al., 2022; Su et al., 2022). Given that SCMV also belongs to the +RNA viruses, we speculate that UN1 cells may be critical for generating SCMV resistance.

### Differences in viral accumulation levels among cell types

In this study, viral accumulation levels varied greatly among cell types, potentially due to specific physiological differences. According to previous studies, photosynthesis-related genes such as *Aspartate transaminase* (*AspAT*, *Zm00001d016198*), *pyruvate, Pi dikinase* (*PPDK*, *Zm00001d038163*), *carbonic anhydrase* (*CA*, *Zm00001d044099*), and *phosphoenolpyruvate carboxylase* (*PEPC*, *Zm00001d046170*) display their lowest expression levels at the leaf base. The leaf base contains relatively young cells at early developmental stages, whereas the leaf tip contains cells at more mature stages (Pick et al., 2011; Tao et al., 2022). Based on the expression levels of these genes among the cells in the four types we identified (Supplemental Figure 2B), we infer that MS4 and UN1 cells are located in the most basal part of maize leaves. Consistent with this, our developmental trajectory analysis showed that MS4 cells form the initial point of leaf tissue development and are positioned at the leaf base, serving as the SCMV infection front. Furthermore, genes expressed in MS4 cells were enriched for translation and for biosynthetic and metabolic processes (Figure 1E). Their location, combined with these physiological factors, likely explains why MS4 cells showed the highest viral accumulation levels and infection rates. On the other hand, the inference that UN1 cells are located at the leaf base is inconsistent with results from our developmental trajectory analysis, as UN1 cells are the most differentiated (Figure 5). However, when combined with our finding that UN1 cells showed the lowest infection rate with SCMV, we speculate that UN1 cells may consist of SCMV-resistant cells at the infection front that suppress viral infection. Unfortunately, *in situ* hybridization of UN-specific marker genes did not confirm the precise localization of UN cells.

### Overlap of up-regulated DEGs across several comparisons

In plants susceptible to specific viral pathogens due to the absence of *R* genes, viruses elicit a range of responses that exacerbate infections. These responses encompass gene expression changes linked to viral redirection of cellular processes and host defensive reactions (Whitham et al., 2003). Notably, diverse genes are preferentially upregulated in different viral infections, whereas downregulated genes tend to be common across various viruses. In this study, we observed a predominant upregulation of a substantial number of DEGs, consistent with previous bulk transcriptomic data (Jiang et al., 2023). Another study integrated currently available microarray data to analyze gene expression changes in compatible *Arabidopsis*-virus interactions (Postnikova and Nemchinov, 2012). The results demonstrated a greater diversity of upregulated genes compared to repressed genes during viral pathogenesis. Moreover, during the early, pre-symptomatic stages of infection, there is notable induction of an array of genes implicated in both general cellular processes and stress-responsive

## Maize genes altered by viral early systemic infection

pathways. Notably, genes associated with amine biosynthetic processes, aromatic amino acid metabolism, photosynthetic activity and responses to both biotic and abiotic stressors are particularly overrepresented among the activated genes, marking these early phases of infection as critical for the expression of these pathways (Postnikova and Nemchinov, 2012). These results are highly consistent with our findings in the present study. During the initial stages of viral infection, the enhancement of infectivity achieved through upregulation of plant host genes is more significant than the benefits gained from downregulation. However, the deeper molecular mechanisms underlying this phenomenon require further exploration.

Furthermore, we found a large overlap between DEGs for several comparisons (Figure 3C and 3H; Supplemental Tables 4 and 5). These genes are either anti-viral genes that protect plants from viruses or pro-viral genes that assist viruses to break through plant defenses. For example, plant NBR1 has been identified as a cargo receptor for selective autophagy of stress-induced protein aggregates and plays an important role in plant responses to a broad scope of stress conditions, including heat, salt, and drought (Zhang and Chen, 2020). A recent study reported that the transcript and protein levels of NBR1 were substantially upregulated upon turnip mosaic virus infection, suggesting an autophagy response triggered by the virus. Potyviruses antagonize NBR1-mediated antiviral autophagy that targets RNA granules containing the viral RNA-silencing suppressor HC-Pro for degradation (Hafrén et al., 2018). Thioredoxins are protein-disulfide reductases with a variety of functions related to REDOX homeostasis. Specific roles of TRX-h in plants include the reduction of purothionin, as well as early signaling in seed germination (Buchanan et al., 1994). In addition, ZmTrxh, which lacks disulfide bond oxidoreductase activity, acts as a molecular chaperone to confer resistance to SCMV at the early infection stage by inhibiting the accumulation of SCMV RNA (Liu et al., 2017).

The observed similarity in DEGs between our comparisons may result from cell-to-cell communication, where cells recognize signals from adjacent cells or the surrounding environment and transform these signals into various molecular functions within the cell. The responses of the cell, along with those of its neighboring cells, in turn cause a series of physiological activities to comprehensively adjust and align with the external environment (Bloemendaal and Kuck, 2013). For example, plasmodesmata connect adjacent cells and regulate the transmission of signaling molecules during cell differentiation and tissue development in higher plants (Lucas et al., 2009). When a potential pathogen enters the host apoplast, danger signals such as heat-shock proteins, nucleotides, reactive oxygen intermediates, and extracellular matrix breakdown products can be sensed by neighboring cells through intercellular signaling (Tabassum and Blilou, 2022). In our study system, plant cells recognize the invasion of SCMV and immediately transmit this information to neighboring cells through efficient intercellular communication. This results in bystander cells being prepared to respond to SCMV in advance, which ensures that the plant can continue to develop during infection. Conversely, it may be possible that SCMV exploits host cell-to-cell communication to engender better conditions for viral replication and survival.

## Plant Communications

In summary, our experimental results offer valuable scRNA transcriptomic insights into interactions between maize and SCMV at early stages of systemic infection. Although we are limited to assessing tissue samples from a single time point, this particular time point is crucial as it represents the initial phase of systemic infection in plant viruses, preceding the manifestation of symptoms and thus playing a pivotal role in the successful establishment of systemic infection. This study offers the first evidence of significant differential responses to SCMV among cell types and successfully identifies antiviral (UN1) and virus-susceptible (MS4 and BS) cell populations, with further analysis of their molecular functions. Through analysis of many DEGs either between cell types or in infected cells with distinct viral accumulation levels compared to bystander cells, we have listed and identified potential anti- or pro-viral factors for SCMV systemic infection. Notably, we identified four genes that play crucial roles in anti- or pro-viral processes during viral infection. Taken together, this study offers resources for anti-SCMV strategies and control of MDMD, and provides a theoretical basis for future studies.

## MATERIALS AND METHODS

### Plant materials and virus inoculation

Seeds of maize (inbred line B73) were germinated in darkness at 25°C for 3 days and transferred to soil, which consisted of a 1.5:1 mixture of soil nutrients and vermiculite. The plants were subsequently grown in a growth chamber with a day temperature of 25°C and a night temperature of 22°C, under light and dark cycles of 16 and 8 h, respectively.

For inoculation, SCMV-GFP was propagated in maize seedlings. Crude virus extracts were prepared by homogenizing symptomatic maize leaf tissues in 0.01 M phosphate buffer (pH 7.0) at a 1:1 (w/v) ratio. The extracts were then inoculated onto the second leaves of 8-day-old maize seedlings.

### Preparation of maize protoplasts

The basal regions of 1 SLs from 20 maize seedlings (inbred line B73) were collected at 2 h on 5 dpi (a pre-symptomatic infection stage, described in Jiang et al., 2023), and dissected into approximately 1-mm filaments using a blade for protoplast preparation. The filaments were immediately immersed in an enzymolysis solution (1.5% Cellulase R-10 [w/v], 0.3% Macerozyme R-10 [w/v], 0.6 M mannitol, 10 mM CaCl<sub>2</sub>, 0.1% bovine serum albumin [w/v], and 10 mM MES). After a 30-min vacuum treatment, tissue digestion was performed at 40 rpm for 4 h at 25°C in the dark. The cell suspension was then filtered through a 35-μm nylon filter and protoplasts were collected by centrifugation at 150 g for 2 min at room temperature. The supernatant was gently removed. The quality of the protoplasts was assessed by observing the morphology of living and dead protoplasts with a hemocytometer under an optical microscope.

### ScRNA-seq library construction and sequencing

Protoplast suspensions from maize leaves were loaded into a 10× Genomics Chromium Controller to generate single-cell gel beads in emulsion using a Chromium Single Cell 3' Reagent Kit version 3. Barcoded cDNA amplification was performed with temperature cycles of 45 min at 53°C and 5 min at 85°C. scRNA-seq libraries were prepared using a Chromium Single Cell 3' Gel Bead and Library Kit and subsequently sequenced on a NovaSeq 6000 (Illumina).

### Generation of single-cell expression matrices

To generate the gene expression matrix of single cells, raw reads were mapped to the maize B73 reference genome (Zm-B73-REFERENCE-NAM-5.0) using Cell Ranger 6.1.1 software provided by the 10×

## Plant Communications

Genomics website ([Bezrutczyk et al., 2021](#)). The B73 reference genome and annotation files were downloaded from Ensembl (<ftp://ftp.ensemblgenomes.org/pub/plants/release-42>). The gene annotation (GTF) file was filtered using the “cellranger mkgtf” function with the “attribute = gene\_biotype: protein\_coding” argument. The “cellranger mkref” function of Cell Ranger was used to build a reference. The “cellranger count” function was performed to generate a raw count matrix.

### Cell clustering and annotation

Data preprocessing, dimensionality reduction, data integration, cell clustering, marker gene identification, and visualization were performed primarily using the R package Seurat (4.0.1) which was also used for subsequent UMI count matrix processing. To exclude cells with low mRNA counts (nFeature\_RNA) and doublets, the data were filtered using the criterion “nFeature\_RNA >400 & nFeature\_RNA <7500 & percent.mt < 20 & percent.pt < 20”. Each dataset was scaled and normalized separately using SCTransform. Integration was performed using nfeatures = 2000, utilizing all features (genes) to find anchors.

Further clustering and annotation were performed on the “integrated” dataset. The data were scaled with the “ScaleData” function in Seurat. The 2000 most highly variable genes were used for dimensionality reduction through principal-component analysis. Based on an elbow plot, the first 20 principal components were used for cell clustering at a resolution of 0.15 according to a shared nearest neighbor graph constructed with “FindNeighbors.” The clusters were visualized and explored using nonlinear dimensionality reduction algorithms (UMAP). Cluster-enriched genes (cluster-specific marker genes) were computed using the function “FindAllMarkers” with the options “test.use = wilcox” and “logfc.threshold = 0.5”.

To assign the cell clusters from scRNA-seq to known cell types, we referenced the expression of known cell-type-specific marker genes from previous studies ([Bezrutczyk et al., 2021](#); [Sun et al., 2022](#); [Tao et al., 2022](#)). For hierarchical clustering, pairwise Pearson’s correlation between each cluster was calculated based on the mean expression of each gene across all cells in the cluster.

### Detection and processing of scRNA-seq data including viral RNA

To identify single cells containing viral RNA, Cell Ranger was used to align raw scRNA-seq reads to a customized reference genome, in which the SCMV genome (NC\_003398.1, NCBI RefSeq) was added as an additional chromosome to the maize reference genome. Single cells with viral reads (UMI  $\geq 0$ ) were retained. Individual cells were sorted according to the levels of viral loads, which conformed to a Poisson distribution.

Ambient SCMV RNAs affected the accurate identification of infected cells. We first selected droplets containing only beads and no cells as a background, with total UMIs ranging from 80 to 400. The viral UMIs in the background were then obtained, nearly meeting a normal distribution. By calculating the 95% confidence interval, the interference of ambient viral UMIs was eliminated. Cells with more than 34 viral UMIs were defined as infected cells, while those with fewer than 34 were classified as bystander cells.

### In situ hybridization

*In situ* hybridization was performed as described previously ([Zhang et al., 2013](#)). dsDNA was amplified by PCR using gene-specific primers containing the T7 RNA polymerase binding site. The corresponding purified PCR products served as templates to generate digoxigenin-labeled antisense and sense RNA probes using the DIG RNA Labeling Mix (Roche) and T7 RNA polymerase (Promega). The gene primer pairs are listed in [Supplemental Table 9](#). The hybridized probes were detected and visualized using an anti-digoxigenin-AP antibody, 4-nitroblue tetrazolium

## Maize genes altered by viral early systemic infection

chloride, and 5-bromo-4-chloro-3-indolyl-phosphate (NBT/BCIP) in the DIG Nucleic Acid Detection Kit (Roche).

### Identifying DEGs between two groups

DEGs across clusters or subclusters were identified by comparing the average normalized mRNA counts in cells of a given cluster with those in all other clusters using the Seurat function “FindMarkers.” Genes with an adjusted *p*-value  $< 0.05$  and a  $\log_2$  fold-change  $\geq 0.5$  were considered significant DEGs.

### Functional enrichment analysis

GO term enrichment analyses were performed with AgriGO-v2 and KEGG pathway enrichment identified significantly overrepresented pathways using hypergeometric tests. Significant enrichment results were visualized with the ggplot2 package (v.3.4.2) ([Wickham, 2016](#)) in R (v.4.1.2).

### Identifying maize genes that show correlation of expression with viral accumulation levels

Only infected cells were used in the expression correlation analysis. Pearson’s correlation analysis was used to analyze the relationship between the expression level of each maize gene and viral accumulation levels. FDR correction was applied to adjusted *p*-values on the correlation coefficients. Host genes were selected if the correlation coefficient  $\rho$  had a value greater than 0.4, an FDR value lower than 0.01, and if they were expressed in at least 10% of cells.

### Clustering maize genes with elevated viral accumulation levels using the Mfuzz package

The Mfuzz package was originally developed as a clustering method for processing gene or protein expression profiling data ([Kumar and E Futschik, 2007](#)). Its core algorithm is based on Fuzzy C-Means Clustering, which analyzes changes in gene or protein expression trends over time. Using the Mfuzz package in R, the expression patterns of maize genes that changed along with elevated viral accumulation levels were grouped into different clusters. These clusters represented the different dynamic patterns of co-variation between maize gene expression levels and viral accumulation levels.

### Pseudotime analysis

Pseudotimes were inferred using the R packages Monocle 2 (v.2.20.0) ([Qiu et al., 2017](#)) and CytoTRACE (v.0.3.3) ([Gulati et al., 2020](#)). Cell types of interest were first subclustered from the Seurat object, then a Monocle object was constructed using the “newCellDataSet” function. The “estimateSizeFactors” and “estimateDispersions” functions in Monocle were used to standardize differences between cells. Next, the top 1000 significant genes, as identified by the “differentialGeneTest” function, were used as ordering genes to construct a single-cell differentiation trajectory. Cells were ordered along a pseudotime axis by the “orderCells” function and the developmental trajectory was visualized using the “plot\_cell\_trajectory” function in Monocle. CytoTRACE was implemented with default parameters. A consensus pseudotime was derived by averaging CytoTRACE- and scVelo-inferred latent times.

### RNA velocity analysis

To understand the continuous changes between individual cell types, RNA velocities were estimated using the velocito package ([La Manno et al., 2018](#)). Expression matrices of unspliced and spliced mRNA were generated with velocito CLI (v.0.17.17) according to the CLI usage guide (velocito run10x). The generated loom files were then processed with a standard CellRank pipeline ([https://cellrank.readthedocs.io/en/stable/cellrank\\_basics.html](https://cellrank.readthedocs.io/en/stable/cellrank_basics.html)). To estimate RNA velocity, cells not used in the pseudotime ordering analysis and genes with insufficient spliced/unspliced counts were filtered out. The data were then normalized and restricted to the top 2000 most highly variable genes using the function “scv.pp.filter\_and\_normalize (min\_shared\_counts = 30, n\_top\_genes = 2000)”. The dynamical model from scVelo was used to estimate RNA

velocities. Initial and terminal states and fate probabilities for the dynamic process of mesophyll development were computed using CellRank (Lange et al., 2022).

#### Virus induced gene silencing (VIGS) in maize using CMV vectors

For the CMV-based virus-induced gene silencing assay, DNA fragments (200–300 bp) representing partial sequences of *ZmSAM-Mt*, *ZmCDF1*, *ZmCC7*, or *ZmPLT1* were individually amplified by RT-PCR using specific primers (Supplemental Table 9) as previously reported (Wang et al., 2016b). The resulting fragments were cloned into the pCMV201-2b<sub>N81</sub> vector to produce vectors pCMV201-2b<sub>N81</sub>-SAM-Mt, pCMV201-2b<sub>N81</sub>-CDF1, pCMV201-2b<sub>N81</sub>-CC7, and pCMV201-2b<sub>N81</sub>-PLT1. All constructs were verified by sequencing prior to use.

*Agrobacterium* cultures carrying pCMV101, pCMV301, or one of the five new plasmids (pCMV201-2b<sub>N81</sub>-SAM-Mt, pCMV201-2b<sub>N81</sub>-CDF1, pCMV201-2b<sub>N81</sub>-CC7, pCMV201-2b<sub>N81</sub>-PLT1, and pCMV201-2b<sub>N81</sub>-GUS) were mixed at a 1:1:1 ratio and infiltrated into the leaves of *Nicotiana benthamiana* plants. Four days later, crude extracts from the infiltrated leaves were individually sap-inoculated into maize B73 seeds using a vascular puncture inoculation technique. Subsequently, the samples were collected for virus detection at 2 h on 5 dpi of SCMV.

#### Recombinant SCMV infectious clones for gene expression in maize

For gene overexpression assays, the GFP fragment in the pSCMV-GFP vector was replaced with the coding sequence of FLAG-tagged *ZmSAM-Mt*, *ZmCDF1*, *ZmCC7*, or *ZmPLT1* to obtain the reconstructed vectors using specific primers (Supplemental Table 9), leading to the generation of the pSCMV-SAM-Mt-FLAG, pSCMV-CDF1-FLAG, pSCMV-CC7-FLAG, and pSCMV-PLT1-FLAG constructs. All constructs were verified by sequencing prior to use.

*Agrobacterium* cultures containing the corresponding SCMV clones were mixed with cultures expressing the viral RNA-silencing suppressor p22 of tomato chlorotic virus and infiltrated into *N. benthamiana* leaves. Subsequently, crude extracts from the infiltrated *N. benthamiana* leaves were used to mechanically inoculate the first true leaf of two-leaf stage maize plants (Xie et al., 2024). The samples were collected at 2 h on 5 dpi for virus detection.

#### DATA AND CODE AVAILABILITY

The data that support the findings of this study are available from the corresponding author upon reasonable request. The raw data have been deposited in the National Genomics Data Center (<https://www.ncbi.ac.cn/>) under accession number [CRA014755](#).

#### FUNDING

This study was supported by grants from the National Natural Science Foundation of China (grant 32072384, W2412104) and the China Agriculture Research System of MOF and MARA (CARS-02). This study was also supported by the Ministry of Agriculture and Rural Affairs of China (NK2023070202). S.C.G. is supported by startup funds from the University of California, Riverside, and by a grant from the National Institute of General Medical Sciences of the National Institutes of Health (award no. R35GM151194).

We gratefully acknowledge the participation of Bestopcell Co., Ltd. (Beijing), for the construction of the single-cell sequencing Library, and thank Jie Liu (Bestopcell, Beijing, China) for his contribution. We are grateful to Shuo Xu, Shuai Yin, Songlin Yang, and Prof. Xingwang Liu (College of Horticulture, China Agricultural University) for their assistance with *in situ* hybridization. We thank Prof. Yule Liu (Tsinghua University, China) for providing the infectious clone of SCMV (pSCMV-GFP).

#### ACKNOWLEDGMENTS

No conflict of interest declared.

#### AUTHOR CONTRIBUTIONS

X.C., S.J., and T.Z. conceived and designed the project. X.C., X.H., K.D., P.W., Q.Y., and L.D. performed the experiments. R.Y., B.L., and Y.Y. performed the bioinformatics analysis. X.C. and T.Z. wrote the manuscript. S.C.G., S.J., and T.Z. revised the manuscript. All authors discussed the results and approved the final manuscript.

#### SUPPLEMENTAL INFORMATION

Supplemental information is available at *Plant Communications Online*.

Received: November 27, 2024

Revised: February 6, 2025

Accepted: March 3, 2025

Published: March 4, 2025

#### REFERENCES

- Abo-Ogiala, A., Carsjens, C., Diekmann, H., Fayyaz, P., Herrfurth, C., Feussner, I., and Polle, A. (2014). Temperature-induced lipocalin (TIL) is translocated under salt stress and protects chloroplasts from ion toxicity. *J. Plant Physiol.* **171**:250–259. <https://doi.org/10.1016/j.jplph.2013.08.003>.
- Alazem, M., He, M.H., Moffett, P., and Lin, N.S. (2017). Abscisic acid induces resistance against bamboo mosaic virus through argonaute 2 and 3. *Plant Physiol.* **174**:339–355. <https://doi.org/10.1104/pp.16.00015>.
- Anjanappa, R.B., Mehta, D., Okoniewski, M.J., Szabelska-Bersewicz, A., Gruissem, W., and Vandeschuren, H. (2018). Molecular insights into cassava brown streak virus susceptibility and resistance by profiling of the early host response. *Mol. Plant Pathol.* **19**:476–489. <https://doi.org/10.1111/mpp.12565>.
- Anzi, C., Pelucchi, P., Vazzola, V., Murgia, I., Gomarasca, S., Piccoli, M.B., and Morandini, P. (2008). The proton pump interactor (*Ppi*) gene family of *Arabidopsis thaliana*: expression pattern of *Ppi1* and characterisation of knockout mutants for *Ppi1* and 2. *Plant Biol.* **10**:237–249. <https://doi.org/10.1111/j.1438-8677.2007.00022.x>.
- Bai, Y., Liu, H., Lyu, H., Su, L., Xiong, J., and Cheng, Z.M. (2022). Development of a single-cell atlas for woodland strawberry (*Fragaria vesca*) leaves during early *Botrytis cinerea* infection using single cell RNA-seq. *Hortic. Res.* **9**:uhab055. <https://doi.org/10.1093/hr/uhab055>.
- Balistreri, G., Horvath, P., Schweingruber, C., Zünd, D., McInerney, G., Merits, A., Mühlmann, O., Azzalin, C., and Helenius, A. (2014). The host nonsense-mediated mRNA decay pathway restricts mammalian RNA virus replication. *Cell Host Microbe* **16**:403–411. <https://doi.org/10.1016/j.chom.2014.08.007>.
- Bergen, V., Soldatov, R.A., Kharchenko, P.V., and Theis, F.J. (2021). RNA velocity-current challenges and future perspectives. *Mol. Syst. Biol.* **17**:e10282. <https://doi.org/10.1525/msb.202110282>.
- Bergen, V., Lange, M., Peidli, S., Wolf, F.A., and Theis, F.J. (2020). Generalizing RNA velocity to transient cell states through dynamical modeling. *Nat. Biotechnol.* **38**:1408–1414. <https://doi.org/10.1038/s41587-020-0591-3>.
- Bezrutczyk, M., Zöllner, N.R., Kruse, C.P.S., Hartwig, T., Lautwein, T., Köhrer, K., Frommer, W.B., and Kim, J.Y. (2021). Evidence for phloem loading via the abaxial bundle sheath cells in maize leaves. *Plant Cell* **33**:531–547. <https://doi.org/10.1093/plcell/koaa055>.
- Bloemendaal, S., and Kück, U. (2013). Cell-to-cell communication in plants, animals, and fungi: a comparative review. *Naturwissenschaften* **100**:3–19. <https://doi.org/10.1007/s00114-012-0988-z>.
- Bost, P., Giladi, A., Liu, Y., Bendjelal, Y., Xu, G., David, E., Blecher-Gonen, R., Cohen, M., Medaglia, C., Li, H., et al. (2020). Host-viral

## Plant Communications

- infection maps reveal signatures of severe COVID-19 patients. *Cell* **181**:1475–1488.e12. <https://doi.org/10.1016/j.cell.2020.05.006>.
- Braidwood, L., Müller, S.Y., and Baulcombe, D.** (2019). Extensive recombination challenges the utility of sugarcane mosaic virus phylogeny and strain typing. *Sci. Rep.* **9**:20067. <https://doi.org/10.1038/s41598-019-56227-y>.
- Buchanan, B.B., Schürmann, P., Decottignies, P., and Lozano, R.M.** (1994). Thioredoxin: a multifunctional regulatory protein with a bright future in technology and medicine. *Arch. Biochem. Biophys.* **314**:257–260. <https://doi.org/10.1006/abbi.1994.1439>.
- Buono, R.A., Paez-Valencia, J., Miller, N.D., Goodman, K., Spitzer, C., Spalding, E.P., and Otegui, M.S.** (2016). Role of SKD1 regulators LIP5 and IST1-LIKE1 in endosomal sorting and plant development. *Plant Physiol.* **171**:251–264. <https://doi.org/10.1104/pp.16.00240>.
- Cabanillas, D.G., Jiang, J., Movahed, N., Germain, H., Yamaji, Y., Zheng, H., and Laliberté, J.F.** (2018). Turnip mosaic virus uses the SNARE protein VTI11 in an unconventional route for replication vesicle trafficking. *Plant Cell* **30**:2594–2615. <https://doi.org/10.1105/tpc.18.00281>.
- Calil, I.P., and Fontes, E.P.B.** (2017). Plant immunity against viruses: antiviral immune receptors in focus. *Ann. Bot.* **119**:711–723. <https://doi.org/10.1093/aob/mcw200>.
- Cao, Y., Ma, J., Han, S., Hou, M., Wei, X., Zhang, X., Zhang, Z.J., Sun, S., Ku, L., Tang, J., et al.** (2023). Single-cell RNA sequencing profiles reveal cell type-specific transcriptional regulation networks conditioning fungal invasion in maize roots. *Plant Biotechnol. J.* **21**:1839–1859. <https://doi.org/10.1111/pbi.14097>.
- Carvalho, A.d.O., and Gomes, V.M.** (2007). Role of plant lipid transfer proteins in plant cell physiology-a concise review. *Peptides* **28**:1144–1153. <https://doi.org/10.1016/j.peptides.2007.03.004>.
- Frenette Charron, J.B., Breton, G., Badawi, M., and Sarhan, F.** (2002). Molecular and structural analyses of a novel temperature stress-induced lipocalin from wheat and *Arabidopsis*. *FEBS Lett.* **517**:129–132. [https://doi.org/10.1016/S0014-5793\(02\)02606-6](https://doi.org/10.1016/S0014-5793(02)02606-6).
- Chi, W.T., Fung, R.W.M., Liu, H.C., Hsu, C.C., and Charng, Y.Y.** (2009). Temperature-induced lipocalin is required for basal and acquired thermotolerance in *Arabidopsis*. *Plant Cell Environ.* **32**:917–927. <https://doi.org/10.1111/j.1365-3040.2009.01972.x>.
- Cho, S.M., Shin, S.H., Kim, K.S., Kim, Y.C., Eun, M.Y., and Cho, B.H.** (2004). Enhanced expression of a gene encoding a nucleoside diphosphate kinase 1 (OsNDPK1) in rice plants upon infection with bacterial pathogens. *Mol. Cells* **18**:390–395. <https://doi.org/10.1016/j.molcel.2004.04.020>.
- Cuperus, J.T.** (2022). Single-cell genomics in plants: current state, future directions, and hurdles to overcome. *Plant Physiol.* **188**:749–755. <https://doi.org/10.1093/plphys/kiab478>.
- Delannoy, E., Batardiere, B., Pateyron, S., Soubigou-Taconnat, L., Chiquet, J., Colcombet, J., and Lang, J.** (2023). Cell specialization and coordination in *Arabidopsis* leaves upon pathogenic attack revealed by scRNA-seq. *Plant Commun.* **4**:100676. <https://doi.org/10.1016/j.xplc.2023.100676>.
- Dielen, A.S., Badaoui, S., Candresse, T., and German-Retana, S.** (2010). The ubiquitin/26S proteasome system in plant-pathogen interactions: a never-ending hide-and-seek game. *Mol. Plant Pathol.* **11**:293–308. <https://doi.org/10.1111/j.1364-3703.2009.00596.x>.
- Dimaano, C., Jones, C.B., Hanono, A., Curtiss, M., and Babst, M.** (2008). Ist1 regulates Vps4 localization and assembly. *Mol. Biol. Cell* **19**:465–474. <https://doi.org/10.1091/mbc.e07-08-0747>.
- Dooki, A.D., Mayer-Posner, F.J., Askari, H., Zaiee, A.A., and Salekdeh, G.H.** (2006). Proteomic responses of rice young panicles to salinity. *Proteomics* **6**:6498–6507. <https://doi.org/10.1002/pmic.200600367>.
- Maize genes altered by viral early systemic infection**
- Dorion, S., and Rivoal, J.** (2015). Clues to the functions of plant NDK isoforms. *N-S Arch Pharmacol* **388**:119–132. <https://doi.org/10.1007/s00210-014-1009-x>.
- Du, K.T., Jiang, T., Chen, H., et al.** (2020). Viral perturbation of alternative splicing of a host transcript benefits infection. *Plant Physiol.* **184**:1514–1531. <https://doi.org/10.1104/pp.20.00903>.
- Fan, Z.F., Chen, H.Y., Liang, X.M., and Li, H.F.** (2003). Complete sequence of the genomic RNA of the prevalent strain of a potyvirus infecting maize in China. *Arch. Virol.* **148**:773–782. <https://doi.org/10.1007/s00705-002-0964-6>.
- Fontes, E.P.B., Teixeira, R.M., and Lozano-Durán, R.** (2021). Plant virus-interactions: unraveling novel defense mechanisms under immune-suppressing pressure. *Curr. Opin. Biotechnol.* **70**:108–114. <https://doi.org/10.1016/j.copbio.2021.03.007>.
- Gao, X.R., Du, Z.C., Hao, K.Q., et al.** (2024). ZmmiR398b negatively regulates maize resistance to sugarcane mosaic virus infection by targeting ZmCSD2/4/9. *Mol. Plant Pathol.* **25**:e13462. <https://doi.org/10.1111/mpp.13462>.
- Gao, R.M., Ng, F.K.L., Liu, P., and Wong, S.M.** (2012). Hibiscus chlorotic ringspot virus coat protein upregulates sulfur metabolism genes for enhanced pathogen defense. *Mol. Plant Microbe Interact.* **25**:1574–1583. <https://doi.org/10.1094/Mpmi-08-12-0203-R>.
- Gao, P., Wang, P., Du, B., Li, P., and Kang, B.H.** (2022). Accelerated remodeling of the mesophyll-bundle sheath interface in the maize C4 cycle mutant leaves. *Sci. Rep.* **12**:5057–5071. <https://doi.org/10.1038/s41598-022-09135-7>.
- Garcia, D., Garcia, S., and Voinnet, O.** (2014). Nonsense-mediated decay serves as a general viral restriction mechanism in plants. *Cell Host Microbe* **16**:391–402. <https://doi.org/10.1016/j.chom.2014.08.001>.
- Guillotin, B., Rahni, R., Passalacqua, M., Mohammed, M.A., Xu, X., Raju, S.K., Ramírez, C.O., Jackson, D., Groen, S.C., Gillis, J., and Birnbaum, K.D.** (2023). A pan-grass transcriptome reveals patterns of cellular divergence in crops. *Nature* **617**:785–791. <https://doi.org/10.1038/s41586-023-06053-0>.
- Guilat, G.S., Sikandar, S.S., Wesche, D.J., Manjunath, A., Bharadwaj, A., Berger, M.J., Ilagan, F., Kuo, A.H., Hsieh, R.W., Cai, S., et al.** (2020). Single-cell transcriptional diversity is a hallmark of developmental potential. *Science* **367**:405–411. <https://doi.org/10.1126/science.aax0249>.
- Hafren, A., Üstün, S., Hochmuth, A., Svensson, S., Johansen, T., and Hofius, D.** (2018). Turnip mosaic virus counteracts selective autophagy of the viral silencing suppressor HC-Pro. *Plant Physiol.* **176**:649–662. <https://doi.org/10.1104/pp.17.01198>.
- Hajheidari, M., Abdollahian-Noghabi, M., Askari, H., Heidari, M., Sadeghian, S.Y., Ober, E.S., and Salekdeh, G.H.** (2005). Proteome analysis of sugar beet leaves under drought stress. *Proteomics* **5**:950–960. <https://doi.org/10.1002/pmic.200401101>.
- He, X.Y., Sambe, M.A.N., Zhuo, C.L., Tu, Q.H., and Guo, Z.F.** (2015). A temperature induced lipocalin gene from *Medicago falcata* (*MfTIL1*) confers tolerance to cold and oxidative stress. *Plant Mol. Biol.* **87**:645–654. <https://doi.org/10.1007/s11103-015-0304-3>.
- Höller, K., Király, L., Künstler, A., Müller, M., Gullner, G., Fattinger, M., and Zechmann, B.** (2010). Enhanced glutathione metabolism is correlated with sulfur-induced resistance in tobacco mosaic virus-infected genetically susceptible *Nicotiana tabacum* plants. *Mol. Plant Microbe Interact.* **23**:1448–1459. <https://doi.org/10.1094/Mpmi-05-10-0117>.
- Ji, J., Du, S., Wang, K., Qi, Z., Zhang, C., Wang, R., Bruening, G., Wang, P., Duanmu, D., and Fan, Q.** (2024). Cowpea lipid transfer protein 1 regulates plant defense by inhibiting the cysteine protease of

## Maize genes altered by viral early systemic infection

cowpea mosaic virus. Proc. Natl. Acad. Sci. USA **121**:e2403424121. <https://doi.org/10.1073/pnas.2403424121>.

Jiang, T., Du, K.T., Xie, J.P., et al. (2023). Activated malate circulation contributes to the manifestation of light-dependent mosaic symptoms. *Cell Rep.* **42**:112333. <https://doi.org/10.1016/j.celrep.2023.112333>.

Jiang, J.X., and Zhou, X.P. (2002). Maize dwarf mosaic disease in different regions of China is caused by sugarcane mosaic virus. *Arch. Virol.* **147**:2437–2443. <https://doi.org/10.1007/s00705-002-0890-7>.

Jiang, T., Du, K., Wang, P., Wang, X., Zang, L., Peng, D., Chen, X., Sun, G., Zhang, H., Fan, Z., et al. (2022). Sugarcane mosaic virus orchestrates the lactate fermentation pathway to support its successful infection. *Front. Plant Sci.* **13**:1099362. <https://doi.org/10.3389/fpls.2022.1099362>.

Jiao, Z.Y., Tian, Y.Y., Wang, J., Ismail, R.G., Bondok, A., and Fan, Z.F. (2022). Advances in research on maize lethal necrosis, a devastating viral disease. *Phytopathol. Res.* **4**:14–24. <https://doi.org/10.1186/s42483-022-00117-1>.

Jin, J., She, Y.Y., Qiu, P., et al. (2022). The cap-snatching frequency of a plant bunyavirus from nonsense mRNAs is low but is increased by silencing of UPF1 or SMG7. *Mol. Plant Pathol.* **23**:576–582. <https://doi.org/10.1111/mpp.13179>.

Kannan, M., Ismail, I., and Bunawan, H. (2018). Maize dwarf mosaic virus: from genome to disease management. *Viruses* **10**:492. <https://doi.org/10.3390/v10090492>.

Kannan, M., Zainal, Z., Ismail, I., Baharum, S.N., and Bunawan, H. (2020). Application of reverse genetics in functional genomics of *Potyvirus*. *Viruses* **12**:803. <https://doi.org/10.3390/v12080803>.

Kim, J.Y., Symeonidi, E., Pang, T.Y., Denyer, T., Weidauer, D., Bezrutczyk, M., Miras, M., Zöllner, N., Hartwig, T., Wudick, M.M., et al. (2021). Distinct identities of leaf phloem cells revealed by single cell transcriptomics. *Plant Cell* **33**:511–530. <https://doi.org/10.1093/plcell/koaa060>.

Kotliar, D., Lin, A.E., Logue, J., Hughes, T.K., Khouri, N.M., Raju, S.S., Wadsworth, M.H., 2nd, Chen, H., Kurtz, J.R., Dighero-Kemp, B., et al. (2020). Single-cell profiling of Ebola virus disease *in vivo* reveals viral and host dynamics. *Cell* **183**:1383–1401.e19. <https://doi.org/10.1016/j.cell.2020.10.002>.

Kumar, L., and E Futschik, M. (2007). Mfuzz: A software package for soft clustering of microarray data. *Bioinformation* **2**:5–7. <https://doi.org/10.6026/97320630002005>.

La Manno, G., Soldatov, R., Zeisel, A., Braun, E., Hochgerner, H., Petukhov, V., Lidschreiber, K., Kastriti, M.E., Lönnberg, P., Furlan, A., et al. (2018). RNA velocity of single cells. *Nature* **560**:494–498. <https://doi.org/10.1038/s41586-018-0414-6>.

Laliberté, J.F., and Sanfaçon, H. (2010). Cellular remodeling during plant virus infection. *Annu. Rev. Phytopathol.* **48**:69–91. <https://doi.org/10.1146/annurev-phyto-073009-114239>.

Lange, M., Bergen, V., Klein, M., Setty, M., Reuter, B., Bakhti, M., Lickert, H., Ansari, M., Schniering, J., Schiller, H.B., et al. (2022). CellRank for directed single-cell fate mapping. *Nat. Methods* **19**:159–170. <https://doi.org/10.1038/s41592-021-01346-6>.

Lee, D.G., Ahsan, N., Lee, S.H., Kang, K.Y., Bahk, J.D., Lee, I.J., and Lee, B.H. (2007). A proteomic approach in analyzing heat-responsive proteins in rice leaves. *Proteomics* **7**:3369–3383. <https://doi.org/10.1002/pmic.200700266>.

Li, Y., Jiao, M.T., Li, Y.J., et al. (2021). *Penicillium chrysogenum* polypeptide extract protects tobacco plants from tobacco mosaic virus infection through modulation of ABA biosynthesis and callose priming. *J. Exp. Bot.* **72**:3526–3539. <https://doi.org/10.1093/jxb/erab102>.

## Plant Communications

Li, X.H., Zhang, X.B., Gao, S., et al. (2022). Single-cell RNA sequencing reveals the landscape of maize root tips and assists in identification of cell type-specific nitrate-response genes. *Crop J.* **10**:1589–1600. <https://doi.org/10.1016/j.cj.2022.02.004>.

Liu, Q.Q., Liu, H.H., Gong, Y.Q., et al. (2017). An atypical thioredoxin imparts early resistance to sugarcane mosaic virus in maize. *Mol. Plant* **10**:483–497. <https://doi.org/10.1016/j.molp.2017.02.002>.

Lobaina, D.P., Tarazi, R., Castorino, T., and Vaslin, M.F.S. (2022). The ubiquitin-proteasome system (UPS) and viral infection in plants. *Plants-Basel* **11**:2476–2488. <https://doi.org/10.3390/plants11192476>.

Lucas, W.J., Ham, B.K., and Kim, J.Y. (2009). Plasmodesmata-bridging the gap between neighboring plant cells. *Trends Cell Biol.* **19**:495–503. <https://doi.org/10.1016/j.tcb.2009.07.003>.

Mahuku, G., Lockhart, B.E., Wanjala, B., Jones, M.W., Kimunye, J.N., Stewart, L.R., Cassone, B.J., Sevgen, S., Nyasani, J.O., Kusia, E., et al. (2015). Maize lethal necrosis (MLN), an emerging threat to maize-based food security in sub-Saharan Africa. *Phytopathology* **105**:956–965. <https://doi.org/10.1094/Phyto-12-14-0367-Fi>.

Marand, A.P., Chen, Z., Gallavotti, A., and Schmitz, R.J. (2021). A cis-regulatory atlas in maize at single-cell resolution. *Cell* **184**:3041–3055.e21. <https://doi.org/10.1016/j.cell.2021.04.014>.

Meyer, F. (2016). Viral interactions with components of the splicing machinery. *Prog Mol Biol Transl* **142**:241–268. <https://doi.org/10.1016/bs.pmbts.2016.05.008>.

Moraes, K.C.M. (2010). RNA surveillance: molecular approaches in transcript quality control and their implications in clinical diseases. *Mol. Med.* **16**:53–68. <https://doi.org/10.2119/molmed.2009.00026>.

Muniz Garcia, M.N., Pais, S.M., Tellez-Inon, M.T., and Capiati, D.A. (2011). Characterization of StPPI1, a proton pump interactor from *Solanum tuberosum* L. that is up-regulated during tuber development and by abiotic stress. *Planta* **233**:661–674. <https://doi.org/10.1007/s00425-010-1329-0>.

Nelms, B., and Walbot, V. (2019). Defining the developmental program leading to meiosis in maize. *Science* **364**:52–56. <https://doi.org/10.1126/science.aav6428>.

Ohlson, M.B., Etison, J.L., Wells, A.I., Kumar, A., Jang, S., Ni, C., Xing, C., Buszczak, M., and Schoggins, J.W. (2023). Genome-scale CRISPR screening reveals host factors required for ribosome formation and viral replication. *mBio* **14**:e0012723. <https://doi.org/10.1128/mbio.00127-23>.

Ortiz-Ramirez, C., Guillotin, B., Xu, X., Rahni, R., Zhang, S., Yan, Z., Coqueiro Dias Araujo, P., Demesa-Arevalo, E., Lee, L., Van Eck, J., et al. (2021). Ground tissue circuitry regulates organ complexity in maize and *Setaria*. *Science* **374**:1247–1252. <https://doi.org/10.1126/science.abj2327>.

Pechanova, O., and Pechan, T. (2015). Maize-pathogen interactions: An ongoing combat from a proteomics perspective. *Int. J. Mol. Sci.* **16**:28429–28448. <https://doi.org/10.3390/ijms161226106>.

Pick, T.R., Bräutigam, A., Schlüter, U., Denton, A.K., Colmsee, C., Scholz, U., Fahnenschlitz, H., Pieruschka, R., Rascher, U., Sonnewald, U., and Weber, A.P.M. (2011). Systems analysis of a maize leaf developmental gradient redefines the current C4 model and provides candidates for regulation. *Plant Cell* **23**:4208–4220. <https://doi.org/10.1105/tpc.111.090324>.

Policicova, K., Badurova, L., and Tomaskova, J. (2020). Metabolic reprogramming as a feast for virus replication. *Acta Virol.* **64**:201–215. [https://doi.org/10.4149/av\\_2020\\_210](https://doi.org/10.4149/av_2020_210).

Postnikova, O.A., and Nemchinov, L.G. (2012). Comparative analysis of microarray data in *Arabidopsis* transcriptome during compatible interactions with plant viruses. *Virol. J.* **9**:101. <https://doi.org/10.1186/1743-422X-9-101>.

## Plant Communications

- Qiu, X., Mao, Q., Tang, Y., Wang, L., Chawla, R., Pliner, H.A., and Trapnell, C.** (2017). Reversed graph embedding resolves complex single-cell trajectories. *Nat. Methods* **14**:979–982. <https://doi.org/10.1038/nmeth.4402>.
- Redinbaugh, M.G., and Stewart, L.R.** (2018). Maize lethal necrosis: An emerging, synergistic viral disease. *Annu. Rev. Virol.* **5**:301–322. <https://doi.org/10.1146/annurev-virology-092917-043413>.
- Ryu, K.H., Zhu, Y., and Schiefelbein, J.** (2021). Plant cell identity in the era of single-cell transcriptomics. *Annu. Rev. Genet.* **55**:479–496. <https://doi.org/10.1146/annurev-genet-071719-020453>.
- Salekdeh, G.H., Siopongco, J., Wade, L.J., Ghareyazie, B., and Bennett, J.** (2002). Proteomic analysis of rice leaves during drought stress and recovery. *Proteomics* **2**:1131–1145. [https://doi.org/10.1002/1615-9861\(200209\)2:9](https://doi.org/10.1002/1615-9861(200209)2:9).
- Satterlee, J.W., Strable, J., and Scanlon, M.J.** (2020). Plant stem-cell organization and differentiation at single-cell resolution. *Proc. Natl. Acad. Sci. USA* **117**:33689–33699. <https://doi.org/10.1073/pnas.2018788117>.
- Seo, J.-K., and Kim, K.-H.** (2016). Long-distance movement of viruses in plants. In *Current Research Topics in Plant Virology*, A. Wang and X. Zhou, eds. (Cham, Switzerland: Springer International Publishing), pp. 153–172. [https://doi.org/10.1007/978-3-319-32919-2\\_6](https://doi.org/10.1007/978-3-319-32919-2_6).
- Seyfferth, C., Renema, J., Wendrich, J.R., Eekhout, T., Seurinck, R., Vandamme, N., Blob, B., Saeys, Y., Helariutta, Y., Birnbaum, K.D., and De Rybel, B.** (2021). Advances and opportunities in single-cell transcriptomics for plant research. *Annu. Rev. Plant Biol.* **72**:847–866. <https://doi.org/10.1146/annurev-aplant-081720-010120>.
- Shang, K.J., Xu, Y., Cao, W.L., et al.** (2022). Potato (*Solanum tuberosum* L.) non-specific lipid transfer protein StLTP6 promotes viral infection by inhibiting virus-induced RNA silencing. *Planta* **256**:54–63. <https://doi.org/10.1007/s00425-022-03948-6>.
- Song, S., Wang, J., Zhou, J., et al.** (2024). Single-cell RNA-sequencing of soybean reveals transcriptional changes and antiviral functions of GmGSTU23 and GmGSTU24 in response to soybean mosaic virus. *Plant Cell Environ.* <https://doi.org/10.1111/pce.15164>.
- Su, Y.C., Peng, Q., Ling, H., et al.** (2022). Systematic identification of miRNA-regulatory networks unveils their potential roles in sugarcane response to sorghum mosaic virus infection. *BMC Plant Biol.* **22**:247–265. <https://doi.org/10.1186/s12870-022-03641-6>.
- Sun, G.L., Xia, M.Z., Li, J., et al.** (2022). The maize single-nucleus transcriptome comprehensively describes signaling networks governing movement and development of grass stomata. *Plant Cell* **34**:1890–1911. <https://doi.org/10.1093/plcell/koac047>.
- Swarbreck, D., Ripoll, P.J., Brown, D.A., Edwards, K.J., and Theodoulou, F.** (2003). Isolation and characterisation of two multidrug resistance associated protein genes from maize. *Gene* **315**:153–164. [https://doi.org/10.1016/s0378-1119\(03\)00734-0](https://doi.org/10.1016/s0378-1119(03)00734-0).
- Tabassum, N., and Blilou, I.** (2022). Cell-to-cell communication during plant-pathogen interaction. *Mol. Plant Microbe Interact.* **35**:98–108. <https://doi.org/10.1094/MPMI-09-21-0221-CR>.
- Tao, S.T., Liu, P., Shi, Y.N., et al.** (2022). Single-cell transcriptome and network analyses unveil key transcription factors regulating mesophyll cell development in maize. *Genes* **13**:374–395. <https://doi.org/10.3390/genes13020374>.
- Liang, X.Y., Ma, Z., Ke, Y.H., et al.** (2023). Single-cell transcriptomic analyses reveal cellular and molecular patterns of rubber tree response to early powdery mildew infection. *Plant Cell Environ.* **46**:2222–2237. <https://doi.org/10.1111/pce.14585>.
- van der Linde, K., Mueller, A.N., Hemetsberger, C., Kashani, F., van der Hoorn, R.A.L., and Doehlemann, G.** (2012). The maize cystatin CC9 interacts with apoplastic cysteine proteases. *Plant Signal. Behav.* **7**:1397–1401. <https://doi.org/10.4161/psb.21902>.
- Tian, Y.Y., Jiao, Z.Y., Qi, F.F., et al.** (2024). Maize catalases are recruited by a virus to modulate viral multiplication and infection. *Mol. Plant Pathol.* **25**:e13440. <https://doi.org/10.1111/mpp.13440>.
- Vergnolle, C., Arondel, V., Jolliot, A., and Kader, J.C.** (1992). Phospholipid transfer proteins from higher plants. *Methods Enzymol.* **209**:522–530. [https://doi.org/10.1016/0076-6879\(92\)09063-9](https://doi.org/10.1016/0076-6879(92)09063-9).
- Virlouvet, L., Jacquemot, M.P., Gerentes, D., Corti, H., Bouton, S., Gilard, F., Valot, B., Trouverie, J., Tcherkez, G., Falque, M., et al.** (2011). The ZmASR1 protein influences branched-chain amino acid biosynthesis and maintains kernel yield in maize under water-limited conditions. *Plant Physiol.* **157**:917–936. <https://doi.org/10.1104/pp.111.176818>.
- Wagner, E., and Lykke-Andersen, J.** (2002). mRNA surveillance: the perfect persist. *J. Cell Sci.* **115**:3033–3038. <https://doi.org/10.1023/A:1020212720330>.
- Walter, S., Kahla, A., Arunachalam, C., Perochon, A., Khan, M.R., Scofield, S.R., and Doohan, F.M.** (2015). A wheat ABC transporter contributes to both grain formation and mycotoxin tolerance. *J. Exp. Bot.* **66**:2583–2593. <https://doi.org/10.1093/jxb/erv048>.
- Wang, B., Tseng, E., Regulski, M., Clark, T.A., Hon, T., Jiao, Y., Lu, Z., Olson, A., Stein, J.C., and Ware, D.** (2016a). Unveiling the complexity of the maize transcriptome by single-molecule long-read sequencing. *Nat. Commun.* **7**:11708–11720. <https://doi.org/10.1038/ncomms11708>.
- Wang, S.Y., Wang, X.Y., Li, S.Q., et al.** (2024). Maize lipid droplet-associated protein 2 is recruited by a virus to enhance viral multiplication and infection through regulating cellular fatty acid metabolism. *Plant J.* **119**:2484–2499. <https://doi.org/10.1111/tpj.16934>.
- Wang, R., Yang, X., Wang, N., Liu, X., Nelson, R.S., Li, W., Fan, Z., and Zhou, T.** (2016b). An efficient virus-induced gene silencing vector for maize functional genomics research. *Plant J.* **86**:102–115. <https://doi.org/10.1111/tpj.13142>.
- Washburn, M., Alaniz-Fabián, J., Scroggs, T., and Nelms, B.** (2023). Single-cell RNA-seq of maize meiocytes and pollen grains. *Nat. Protoc.* **18**:3512–3533. <https://doi.org/10.1038/s41596-023-00889-6>.
- Whitham, S.A., Quan, S., Chang, H.S., Cooper, B., Estes, B., Zhu, T., Wang, X., and Hou, Y.M.** (2003). Diverse RNA viruses elicit the expression of common sets of genes in susceptible *Arabidopsis thaliana* plants. *Plant J.* **33**:271–283. <https://doi.org/10.1046/j.1365-313X.2003.01625.x>.
- Wickham, H.** (2016). *ggplot2: Elegant Graphics for Data Analysis* (New York: Springer-Verlag).
- Wolf, F.A., Hamey, F.K., Plass, M., Solana, J., Dahlin, J.S., Göttgens, B., Rajewsky, N., Simon, L., and Theis, F.J.** (2019). PAGA: Graph abstraction reconciles clustering with trajectory inference through a topology preserving map of single cells. *Genome Biol.* **20**:59–67. <https://doi.org/10.1186/s13059-019-1663-x>.
- Wu, G.W., Cui, X.Y., Chen, H., et al.** (2018). Dynamin-like proteins of endocytosis in plants are coopted by potyviruses to enhance virus infection. *J. Virol.* **92**, e01320–18. <https://doi.org/10.1128/jvi.01320-18>.
- Wu, G.W., Cui, X.Y., Dai, Z.J., et al.** (2020). A plant RNA virus hijacks endocytic proteins to establish its infection in plants. *Plant J.* **101**:384–400. <https://doi.org/10.1111/tpj.14549>.
- Xie, J.P., Fei, X.H., Yan, Q., et al.** (2024). The C4 photosynthesis bifunctional enzymes, PDRPs, of maize are co-opted to cytoplasmic viral replication complexes to promote infection of a prevalent potyvirus sugarcane mosaic virus. *Plant Biotechnol. J.* **22**:1812–1832. <https://doi.org/10.1111/pbi.14304>.
- Xu, X.S., Crow, M., Rice, B.R., et al.** (2021). Single-cell RNA sequencing of developing maize ears facilitates functional analysis and trait

## Maize genes altered by viral early systemic infection

candidate gene discovery. Dev. Cell **56**:557–568.e6. <https://doi.org/10.1016/j.devcel.2020.12.015>.

**Xue, M.S., Arvy, N., and German-Retana, S.** (2023). The mystery remains: How do potyviruses move within and between cells? Mol. Plant Pathol. **24**:1560–1574. <https://doi.org/10.1111/mpp.13383>.

**Yang, M., Ismayil, A., and Liu, Y.L.** (2020). Autophagy in plant-virus interactions. Annu. Rev. Virol. **7**:403–419. <https://doi.org/10.1146/annurev-virology-010220-054709>.

**Yang, F.B., Zhang, X.Y., Xue, H., et al.** (2022). (Z)-3-hexenol primes callose deposition against whitefly-mediated begomovirus infection in tomato. Plant J. **112**:694–708. <https://doi.org/10.1111/tpj.15973>.

**Yuan, W., Chen, X., Du, K.T., et al.** (2024). Nla-Pro of sugarcane mosaic virus targets Corn Cysteine Protease 1 (CCP1) to undermine salicylic acid-mediated defense in maize. PLoS Pathog. **20**:e1012086. <https://doi.org/10.1371/journal.ppat.1012086>.

**Yue, H., Chen, G., Zhang, Z., Guo, Z., Zhang, Z., Zhang, S., Turlings, T.C.J., Zhou, X., Peng, J., Gao, Y., et al.** (2024). Single-cell transcriptome landscape elucidates the cellular and developmental responses to tomato chlorosis virus infection in tomato leaf. Plant Cell Environ. **47**:2660–2674. <https://doi.org/10.1111/pce.14906>.

**Zavaliev, R., Ueki, S., Epel, B.L., and Citovsky, V.** (2011). Biology of callose ( $\beta$ -1,3-glucan) turnover at plasmodesmata. Protoplasma **248**:117–130. <https://doi.org/10.1007/s00709-010-0247-0>.

**Zhang, H.S., Yang, H.L., Hu, D.S., et al.** (2021). Single-cell RNA sequencing of meiocytes and microspores reveals the involvement of the *Rf4* gene in redox homeostasis of CMS-C maize. Crop J. **9**:1237–1247. <https://doi.org/10.1016/j.cj.2021.06.012>.

## Plant Communications

**Zhang, Y., and Chen, Z.X.** (2020). Broad and complex roles of NBR1-mediated selective autophagy in plant stress responses. Cells **9**:2562–2577. <https://doi.org/10.3390/cells9122562>.

**Zhang, X.L., Zhou, Y., Ding, L., Wu, Z., Liu, R., and Meyerowitz, E.M.** (2013). Transcription repressor HANABA TARANU controls flower development by integrating the actions of multiple hormones, floral organ specification genes, and GATA3 family genes in *Arabidopsis*. Plant Cell **25**:83–101. <https://doi.org/10.1105/tpc.112.107854>.

**Zhang, J., Zhu, Q.S., Yu, H.J., et al.** (2019). Comprehensive analysis of the cadmium tolerance of abscisic acid-stress- and ripening-induced proteins (ASRs) in maize. Int. J. Mol. Sci. **20**:133–145. <https://doi.org/10.3390/ijms20010133>.

**Zheng, Y., Li, S., Li, S.H., Yu, S., Wang, Q., Zhang, K., Qu, L., Sun, Y., Bi, Y., Tang, F., et al.** (2022). Transcriptome profiling in swine macrophages infected with African swine fever virus at single-cell resolution. Proc. Natl. Acad. Sci. USA **119**:e2201288119. <https://doi.org/10.1073/pnas.2201288119>.

**Zhong, Y., Li, Y., Chen, Z.Z., et al.** (2021). Treatment of *Penicillium chrysogenum* extracts (PDMP) restricts the spread of tobacco mosaic virus by priming callose deposition in *Nicotiana benthamiana*. Physiol. Mol. Plant Pathol. **113**:101569. <https://doi.org/10.1016/j.pmpp.2020.101569>.

**Zhu, F., Cao, M.Y., Zhu, P.X., Zhang, Q.P., and Lam, H.M.** (2023a). Non-specific LIPID TRANSFER PROTEIN 1 enhances immunity against tobacco mosaic virus in *Nicotiana benthamiana*. J. Exp. Bot. **74**:5236–5254. <https://doi.org/10.1093/jxb/erad202>.

**Zhu, J., Lolle, S., Tang, A., Guel, B., Kvitko, B., Cole, B., and Coaker, G.** (2023b). Single-cell profiling of *Arabidopsis* leaves to *Pseudomonas syringae* infection. Cell Rep. **42**:112676. <https://doi.org/10.1016/j.celrep.2023.112676>.